Observations of intermittent deep currents and eddies in the Gulf of Mexico

Nicolas Kolodziejczyk,[1,2] José Ochoa,[1] Julio Candela,[1] and Julio Sheinbaum[1]

Received 17 January 2012; revised 25 July 2012; accepted 26 July 2012; published 14 September 2012.

[1] Intense currents having speeds between 10 and 40 cm.s^{-1} from 1000 m below the surface to the bottom have been measured in the Loop Current (LC) region and in the Western Gulf of Mexico (WGM). The observations come from moored current meters sampling from the near-surface to the bottom at 3300–3500 m and from August 2008 to August 2010. Ten intermittent intensified currents are documented. These events last 10 to 30 days and take place in the region just between the surface-intensified anticyclonic-cyclonic features, as deduced from altimetry and measured currents. In the WGM, they occur between the cores of anticyclone-cyclone pairs. In the Eastern Gulf of Mexico (EGM), they occur in the Loop Current edge between its anticyclonic circulation and a neighboring cyclone. During each event, the analysis shows an increase in the barotropic contribution to the current. In the Loop Current region, these events are often associated with intensification of cyclonic vorticity in the deep layer.

Citation: Kolodziejczyk, N., J. Ochoa, J. Candela, and J. Sheinbaum (2012), Observations of intermittent deep currents and eddies in the Gulf of Mexico, *J. Geophys. Res.*, *117*, C09014, doi:10.1029/2012JC007890.

1. Introduction

[2] In a stratified ocean, characterized by the upper-ocean pycnocline, theoretical studies and numerical simulations favor the idea that mesoscale energy transfer to the barotropic mode is inhibited. The energy of high baroclinic modes cascades preferentially toward the first baroclinic mode, and toward horizontal scales of the same mode. This could explain why surface mesoscale vortices are generally surface-trapped in the ocean [*Smith and Vallis*, 2001, 2002]. Thus, rare are the occasions when the mesoscale flow is mostly barotropic or nearly unidirectional through most of the water column.

[3] During recent moored observations at depths of over 2000 m in the Gulf of Mexico (GM) the upper instruments recorded, via their pressure sensors, vertical excursions of mooring elements exceeding 100 m, which can last more than 10 days. These moorings, when standing vertical, have the uppermost float near 130 m below the surface. However, when the instruments recorded intense horizontal currents over the whole water column or within the deep layer (below 1000 m depth), the mooring elements deepened, in one event up to 400 m. Significant deepening of the mooring elements occurs when the deep flow, which in the Gulf of Mexico is almost always columnar [*Inoue et al.*, 2008, *Welsh and Inoue*, 2000, *Kolodziejczyk et al.*, 2011], is intensified rather than coincidental with intense surface currents. The vertical excursions have nothing to do with upwelling/downwelling water velocities but with the lateral drag (i.e., the horizontal component of the drag) due to the currents. When the deep current contribution is intense, it induces an enhanced drag that pushes the mooring elements sideways. The anchor supports the tension exerted by the connecting element (a chain), which under lateral drag must be tilted. For an oversimplified static model of uniform lateral drag onto a single cable connecting the anchor to a flotation element, the curve should be a catenary. Since the cable length is, for all purposes constant, the flotation element would deepen as the drag increases. The deepest excursion, of ~400 m, occurred when the deep current reached 40 cm.s^{-1}, but in other occasions the same mooring recorded surface currents as strong as 100 cm.s^{-1} and excursions were not as large. The currents under consideration are only the low frequency subinertial contributions. With a set of moored measurements globally distributed, *Wunsch* [1997] also reports similar excursions during barotropic flow and deep flow intensification.

[4] The baroclinic anticyclonic Loop Current Eddies (LCEs) that separate episodically from the Loop Current (LC) in the Eastern Gulf of Mexico (EGM) travel toward the western boundary of the Gulf Mexico (GM), interacting with numerous companion cyclones and contributing significantly to the variability of the upper layer (above 500–1000 m depth) in the central and Western Gulf of Mexico (WGM). Numerous observational studies describe such LCEs, their paths, and interactions with cyclones and bottom topography [e.g., *Merrell and Morrison*, 1981; *Brooks and Legeckis*, 1982; *Vukovich and Waddell*, 1991; *Hamilton*, 1992; *Vidal et al.*, 1992; *Hamilton et al.*, 2002; *Vukovich*, 2007]. There

[1]Departamento de Oceanografía Física, CICESE, Ensenada, Mexico.
[2]LPO/Ifremer/CNRS/IRD/UBO, Plouzane, France.

Corresponding author: N. Kolodziejczyk, LPO/Ifremer/CNRS/IRD/UBO, Centre de Brest, BP 70, F-29263, Plouzané, France. (nicolas.kolodziejczyk@gmail.com)

0148-0227/12/2012JC007890

is also a large volume of numerical studies dealing with the LC and LCEs [e.g., *Hurlburt and Thompson*, 1980; *Oey et al.*, 2005; *Chérubin et al.*, 2006; *Hyun and Hogan*, 2008; *Oey*, 2008].

[5] The observation of deep currents (below 1000 m depth, hereafter referred as the deep layer) is less common than surface flows. Based on historical hydrographic measurements in the GM, *DeHaan and Sturges* [2005] suggest a general cyclonic mean circulation, with speeds of about 2–3 cm.s^{-1} in the deep layer. However, clear evidence of such deep cyclonic circulation remains inconclusive as shown in a recent study of the western Bay of Campeche (BC) [see *Kolodziejczyk et al.*, 2011, Figure 3].

[6] At sub-inertial frequencies and over the continental slopes all around the GM, Topographic Rossby Waves (TRWs) explain most of the variability of deep currents with amplitudes of about 20 cm.s^{-1}. TRWs manifest as unidirectional motions and intensified toward the bottom [*Rhines*, 1970]. They have been identified in observations [*Hamilton*, 1990, 2007, 2009; *Kolodziejczyk et al.*, 2011] and simulated in numerical studies [*Oey and Lee*, 2002; *Oey*, 2008]. These studies suggest that one of the forcing mechanisms for TRWs is deep eddies interacting with bottom topography. In the EGM, several numerical studies [*Hurlburt and Thompson*, 1982; *Oey and Lee*, 2002; *Chérubin et al.*, 2006; *Oey*, 2008] have proposed that baroclinic instability off Campeche Bank and West Florida generates deep cyclones, which also contribute to the LCE shedding process. *Oey and Lee* [2002] and *Oey* [2008] argue that these deep cyclones are in turn the source of TRWs whose periods are nearly 20 days, similar to the observed motions in the northern GM [*Hamilton*, 2007]. Other numerical results [*Hurlburt and Thompson*, 1982; *Welsh and Inoue*, 2000] indicate that deep eddies can be generated by the vertical stretching, consequent with potential vorticity conservation and the translation of LCEs over the deep layer. This type of deep eddy generation has also been described in theoretical studies [*Cushman-Roisin et al.*, 1990].

[7] *Inoue et al.* [2008] observed strong intermittent coherent currents throughout the water column (barotropic currents) below the 'necking point' of the LC during detachment of an LCE. In this kind of detachment, an LC frontal cyclone plays a key role in the 'necking-down' of the LC [*Cochrane*, 1972; *Schmitz*, 2005]. Hydrographical sections across the LC and frontal cyclones show a deep extension of the cyclones, reaching speeds over 10 cm.s^{-1} at 900 m depth [*Cochrane*, 1972; *Vukovich and Maul*, 1985; *Vukovich*, 1986; *Zavala-Hidalgo et al.*, 2003; *Schmitz*, 2005] suggesting a deepening of the currents at the confluence of the LC and the frontal cyclone. However, their hydrographic sections did not extend below 1000 m depth. Hydrographic surveys in the western GM have also revealed the extension of significant speeds deeper than 800 m at the confluence of a cyclone and an anticyclone [*Merrell and Morrison*, 1981; *Brooks and Legeckis*, 1982; *Hamilton*, 1992; *Vidal et al.*, 1992; *Hamilton et al.*, 2002], but these hydrographic data are also limited to the upper 1000 m. *De Ruijter et al.* [2004] observed, a jet extending to 2000 m below the midpoint of a dipole-like vortex in the boundary of the East Madagascar Current in Lowered-ADCP (L-ADCP) measurements. The kind of events discussed in this paper seems to be the first documented with moored current measurements.

[8] Here, observations are presented that show the intensification of currents at depths below 1000 m when the near-surface fields manifest the narrowing of the region between cyclonic and anticyclonic circulations. The intensification of currents, between counter-rotating eddies that approach each other, is not surprising; almost the same transport is maintained as the width narrows. However, the surface eddies barely extend coherently below 1000 m, thus, the intensification of deep flows, sometimes in the same direction as the surface flows, is puzzling.

[9] This paper is organized as follows: section 2 presents currents and hydrographical moored data along with AVISO altimetry maps, focusing at the confluence of cyclonic and anticyclonic surface flows. Section 3 presents a general overview of the different occurrences of intensification of deep currents in the data. In section 4, four examples of such events are described in detail, two in the WGM and two in the EGM. In section 5, the current's vertical structure during these events is discussed, together with a summary of the results.

2. Data

2.1. Moored Data

[10] The velocity data for this study come from 69 current meters distributed on moorings labeled H2, H3, L, A and K (in Figure 1) deployed from August 2008 to July 2010, P deployed from October 2008 to July 2010, and H1 from February 2008 to August 2010. Moorings A, L, K and P were at nearly 3500 m depth and H1, H2 and H3 at 3300 m. Each mooring was deployed for a year and then redeployed for a second consecutive year (Table 1). All moorings were equipped with three ADCPs (Acoustic Doppler Current Profilers) covering from near the surface to about 1000 m depth, point current meters at nominal depths of 1300, 1500, 1700, 2000, 2500, 3000 m, and one downward-looking ADCP near 20 m above the bottom (see Table 1 for details). Given that vertical excursions of the instruments are recorded via pressure gauges, velocities at a given depth level are estimated via interpolations.

[11] The moorings were also instrumented with Microcats, providing temperature and salinity time series with accuracy of 0.003°C and 0.003 PSS respectively. The Microcats were located nominally at 108 m, 161 m, 413 m, 512 m depth for moorings H1, H2 and H3; and at 108 m, 161 m, 413 m, 715 m depth for moorings A, L, K and P (see Figure 1 and Table 1 for more details).

[12] Each time series was filtered with a low-pass Lanczos filter with cut-off frequency of 0.5 cpd (i.e., period of 2 days, hereafter named 2-DLP time series). Thus, inertial (35 h at ~20° latitude) and main tidal frequencies are removed.

2.2. AVISO Products

[13] To infer the surface dynamics in the GM, the AVISO 1/3° × 1/3° gridded daily near real-time Absolute Dynamic Topography (ADT) and surface geostrophic current products have been used. Away from the continental shelves (water depths >200 m depth), these altimetry products provide an accurate estimation of these surface fields. RMS differences between AVISO and available in situ drifting buoy measurements is less than 13 cm.s^{-1} over the Atlantic Ocean and less than 17 cm.s^{-1} over the Gulf Stream area [*Rio and*

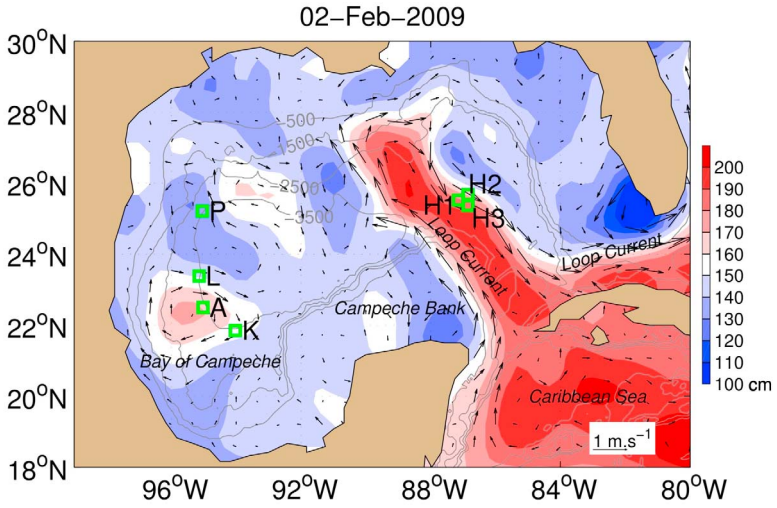

Figure 1. Gulf of Mexico with the position of moorings P, L, A, K, H1, H2, H3. Absolute dynamic topography from AVISO (in cm) is shaded, and the arrows are the surface geostrophic velocities deduced from altimetry (in m.s^{-1}). Isobaths are plotted in gray.

Hernandez, 2004]. This accuracy is sufficient in the present study, since we consider surface velocities of cyclonic and anticyclonic features greater than 20 cm.s^{-1}.

3. Observation of Deep Events

3.1. Velocities

[14] The energetic events observed in the data are summarized in Table 2. These events appear at different places in the GM: in the EGM or LC region at moorings H1, H2 and H3 (Figure 1), in the northwestern part of the GM at mooring P, and north of the BC at moorings L, A and K. The events selected in Table 2 have intensities ranging from 10 cm.s^{-1} to 40 cm.s^{-1} at 2000 m depth (events having speeds less than 10 cm.s^{-1} have not been considered), and last from 10 days up to more than one month. They all appear in association with counter-rotating flows at the surface. Some events are recorded at two or three moorings, for instance at H1, H2 and H3 or at L and A. While moorings H1, H2 and H3 are ~40 km apart from each other, mooring A is 99 (126) km south (north) of L (K). Thus, their horizontal scale is comparable with surface eddy activity at the mesoscale (about 300 km for an LCE).

[15] Figure 2 shows both components of 2-DLP velocity over the whole water column at H1, P and A (between 0 and 3300 m depth for H1 and 0–3500 m for P and A) for the full length of the time series. At H1 (Figures 2a and 2b, H1), five events described in Table 2 (Events 1, 2, 5 and 9) are visible in March 2008, August 2008, December 2008, March 2009 and late August 2009. They are characterized by an increase in speed, mainly in the meridional or V-component and over the whole water column (Figure 2b), whereas the zonal or U-component is weaker (Figure 2a). The V-component reaches more than 90 cm.s^{-1} at the surface during the August 2008 event, and more than 40 cm.s^{-1} at 2000 m depth during the late August 2009 event. Note the large mooring displacements (more than 400 m, in August 2009) identified by the near-surface blanks.

[16] Due to the vertical displacements of the mooring components, the near-surface profilers loose data during each of the strong events. The near-surface blanks shown in Figure 2 are due to the deepening of the ADCP that profiles the near-surface layer; profiling with the same reach but from a variable depth. This is induced by an enhanced lateral drag onto the whole mooring line that sways it from the vertical.

[17] In another example, during January–March 2010, there are drawdowns of the instruments associated with strong surface intensification. The V-component reaches 70 cm.s^{-1} down to 1000 m depth, with a slight intensification in the deepest currents of up to ~5 cm.s^{-1}. In mooring H3 (not shown) several events with speeds greater than 10 cm.s^{-1} from 1000 m depth to the bottom are recorded.

[18] At mooring P (Figures 2c and 2d), events are visible during April 2009 and June 2009 (Events 6 and 7, Table 2). The speeds near the surface reach more than 50 cm.s^{-1}, and more than 10 cm.s^{-1} at 2000 m depth. They are also characterized by the deepening of the moored current meters as manifested by the blanks or absence of data near the surface, but the speed of the events and deepening of the mooring's elements are not as intense as in the EGM.

[19] Deep energetic currents reaching 10 cm.s^{-1} and intensified toward the bottom below 1000 m depth occur in February–March 2009, July to September 2009, and October to March 2009 (Figure 2d). These events appear to be less connected with a surface intensification as, for example, the events in July–September 2009. The deep currents that amplify toward the bottom could be explained by focusing of TRWs as explained by *Hamilton* [2009] near the Perdido Escarpment in the northern corner of WGM. They could also be a manifestation of deep eddies at this location [*Hofmann and Worley*, 1986].

[20] A drawdown occurred at mooring P during May 2010 but in the absence of intense, deep speeds. Although, the currents exhibited the largest near-surface speed (up to 80 cm.s^{-1}),

Table 1. Moorings in the Gulf of Mexico for Both Periods (Legs 1 and 2) of Observation Between 2008 and 2010[a]

Mooring	Period		Latitude, Longitude		Water Depth (m)		Variable	Instrument (Looking)		Instrument Depth (m)		Range Depth (m)		Bin Size (m)
	Leg 1	Leg 2	Leg 1	Leg 2	Leg 1	Leg 2		Leg 1	Leg 2	Leg 1	Leg 2	Leg 1	Leg 2	
H1	Feb 2008–Jul 2009	Jul 2009–Apr 2010	25°22.56′N, 86°51.10′W	25°22.53′N, 86°51.01′W	3329	3330	U,V	WH300 (up)	WH300 (up)	138	142	56–128	20–132	8
							U,V	LR75 (dw)	LR75 (dw)	138	142	163–707	167–679	16
							U,V	LR75 (dw)	LR75 (dw)	544	549	569–1033	573–1005	16
							U,V	Nortek	Nortek	1154	1158			
							U,V	…	Seaguard	…	1338			
							U,V	…	Nortek	…	1574			
							U,V	…	Nortek	…	1830			
							U,V	RCM11	Seaguard	2334	2337			
							U,V	RCM11	Nortek	2841	2845			
							U,V	WH600 (dw)	WH600 (dw)	3310	3314	3312–3320	3313–3327	0.5
							T,S	MicroCat	MicroCat	138	142			
							T,S	MicroCat	MicroCat	191	195			
							T,S	MicroCat	MicroCat	243	247			
							T,S	MicroCat	MicroCat	545	549			
H2	Jul 2008–Jul 2009	Jul 2009–Apr 2010	25°40.90′N, 86°51.40′W	25°41.00′N, 86°51.20′W	3301	3324	U,V	WH300 (up)	WH300 (up)	110	143	28–100	29–133	8
							U,V	LR75 (dw)	LR75 (dw)	110	143	135–679	168–712	16
							U,V	LR75 (dw)	LR75 (dw)	516	550	541–973	575–1039	16
							U,V	Nortek	Seaguard	1126	1159			
							U,V	…	Nortek	…	1339			
							U,V	Nortek	Seaguard	1542	1575			
							U,V	Nortek	Nortek	1798	1831			
							U,V	…	Seaguard	…	2338			
							U,V	…	Nortek	…	2846			
							U,V	WH600 (dw)	WH600 (dw)	3282	3305	3284–3291	3307–3317	0.5
H3	Jul 2008–Jul 2009	Jul 2009–Apr 2010	25°31.64′N, 86°08.51′W	25°31.40′N, 86°08.84′W	3358	3325	U,V	WH300 (up)	WH300 (up)	126	144	36–116	30–134	8
							U,V	LR75 (dw)	LR75 (dw)	126	144	151–727	168–665	16
							U,V	LR75 (dw)	LR75 (dw)	574	551	599–1031	576–1008	16
							U,V	Nortek	Nortek	1183	1060			
							U,V	…	Seaguard	…	1340			
							U,V	Nortek	Nortek	1599	1576			
							U,V	…	Nortek	…	1832			
							U,V	Nortek	Seaguard	2363	2339			
							U,V	…	Nortek	…	2847			
							U,V	WH600 (dw)	WH600 (dw)	3339	3306	3341–3348	3308–3320	0.5
P	Sep 2008–Jul 2009	Jul 2009–Jul 2010	25°12.32′N, 95°02.25′W	25°12.77′N, 95°02.53′W	3528	3519	U,V	WH300 (up)	WH300 (up)	136	128	30–126	30–118	8
							U,V	LR75 (dw)	LR75 (dw)	136	128	131–721	153–729	16
							U,V	LR75 (dw)	LR75 (dw)	743	735	768–1104	760–1128	16
							U,V	Seaguard	Nortek	1352	1344			
							U,V	RCM11	Nortek	1533	1525			
							U,V	RCM11	Nortek	1768	1760			
							U,V	RCM11	Nortek	2024	2016			
							U,V	RCM11	Nortek	2532	2524			
							U,V	RCM11	Nortek	3039	3031			

Table 1. (continued)

Mooring	Period		Latitude, Longitude		Water Depth (m)		Variable	Instrument (Looking)		Instrument Depth (m)		Range Depth (m)		Bin Size (m)
	Leg 1	Leg 2	Leg 1	Leg 2	Leg 1	Leg 2		Leg 1	Leg 2	Leg 1	Leg 2	Leg 1	Leg 2	
							U,V	WH600 (dw)	WH600 (dw)	3508	3500	3511–3518	3502–3516	0.5
							T,S	MicroCat	MicroCat	136	128			
							T,S	MicroCat	MicroCat	189	181			
							T,S	MicroCat	MicroCat	441	433			
							T,S	…	MicroCat	…	735			
L	Sep 2008–Jul 2009	Jul 2009–Jul 2010	23°22.58′N, 95°07.25′W	23°63.92′N, 95°08.56′W	3534	3513	U,V	WH300 (up)	WH300 (up)	143	122	45–133	32–112	8
							U,V	LR75 (dw)	LR75 (dw)	143	122	168–744	147–723	16
							U,V	LR75 (dw)	LR75 (dw)	750	729	775–1159	754–1154	16
							U,V	RCM11	Nortek	1359	1338			
							U,V	RCM11	Nortek	1540	1519			
							U,V	Seaguard	RCM11	1776	1754			
							U,V	RCM11	Nortek	2031	2010			
							U,V	RCM11	RCM11	2539	2518			
							U,V	…	RCM11	…	3025			
							U,V	WH600 (dw)	WH600 (dw)	3515	3494	3518–3525	3496–3507	0.5
A	Jul 2008–Jul 2009	Jul 2009–Jul 2010	22°29.62′N, 95°00.73′W	22°30.33′N, 95°01.29′W	3483	3489	U,V	WH300 (up)	WH300 (up)	92	98	26–82	16–88	8
							U,V	LR75 (dw)	LR75 (dw)	92	98	117–693	123–683	16
							U,V	LR75 (dw)	LR75 (dw)	699	705	724–1076	729–1113	16
							U,V	Nortek	RCM11	1308	1314			
							U,V	Nortek	Nortek	1489	1495			
							U,V	Nortek	RCM11	1980	1730			
							U,V	Nortek	Nortek	1725	1986			
							U,V	Nortek	RCM11	2488	2494			
							U,V	Nortek	RCM11	2995	3001			
							U,V	WH600 (dw)	WH600 (dw)	3464	3470	3466–3474	3472–3485	0.5
							T,S	MicroCat	MicroCat	93	98			
							T,S	MicroCat	MicroCat	145	151			
							T,S	MicroCat	MicroCat	397	403			
							T,S	…	MicroCat	…	705			
K	Jul 2008–Jul 2009	Jul 2009–Jul 2010	21°50.84′N, 94°01.24W	21°50.87′N, 95°01.54′W	3534	3537	U,V	WH300 (up)	WH300 (up)	143	126	61–133	28–116	8
							U,V	LR75 (dw)	LR75 (dw)	143	126	168–648	151–503	16
							U,V	LR75 (dw)	LR75 (dw)	750	733	775–1127	758–1126	16
							U,V	Nortek	Nortek	1359	1342			
							U,V	Seaguard	RCM11	1540	1495			
							U,V	Nortek	Nortek	1776	1778			
							U,V	…	RCM11	…	1986			
							U,V	…	Nortek	…	2542			
							U,V	Nortek	Nortek	3046	3049			
							U,V	WH600 (dw)	WH600 (dw)	3515	3518	3518–3525	3520–3533	0.5

[a]The RCM11 and Seaguard current meter are manufactured by Aanderaa. LR75, WH300, WH600 are ADCPs of 75, 300 KHz and 600 KHz, respectively. 'Up' and 'dw' indicate ADCPs looking upward and downward, respectively. Dots indicate that no data are available during the period.

Table 2. Deep Current Events in the Gulf of Mexico Currentmeters Records[a]

Event	Mooring	Maximum Speed at 2000 m Depth ($cm.s^{-1}$)	Period	Approximately Duration (days)	Situation at the Surface
1	H1	32	Mar 2008	10	Interaction between a cyclone and LC north of Campeche Bank
2	H1,H2,H3	30	Aug 2008	15	Interaction between a cyclone and LC north of Campeche Bank
3	**H1,H2,H3**	26	Dec 2008	20	Interaction between a cyclone and LCE west of Florida
4	**A,L**	20	Feb 2009	30	Interaction between a cyclone and the LCE CAMERON in north of Bay of Campeche
5	H1,H2,H3	28	Mar 2009	15	Small cyclones north of Campeche Bank and west of Florida 'necking' a LC
6	P	10	Apr 2009	12	Interaction between a cyclone with small anticyclone in the northwestern corner of GM
7	P	10	Jun 2009	15	LCE DARWIN arriving in the northwestern corner of GM and interacts with a cyclone
8	**A,L,K**	16	Aug 2009	30	Interaction between a cyclone and the LCE DARWIN in north of Bay of Campeche
9	**H1,H2,H3**	40	Sep 2009	12	Cyclones north of Campeche Bank and west of Florida 'necking' a LCE
10	A	16	Oct 2009	5	Interaction between a cyclone and LCE DARWIN at north of the Bay of Campeche

[a]Bold mooring numbers indicate events described in text. The names of the LCEs (CAMERON, DARWIN) are defined by Horizon Marine Inc. (http://www.horizonmarine.com/loop_current_Eddies.php).

the deepening of the mooring was not as intense as during the "events" at the mooring.

[21] At mooring A (Figures 2e and 2f), the deep layer energy is mainly explained by the presence of three energetic events (4, 8 and 10, Table 2); one occurring in February 2009 with speeds exceeding 20 $cm.s^{-1}$ at 2000 m and 50 $cm.s^{-1}$ just below the surface, and two others during August and October 2009 with a maximum velocity of 16 $cm.s^{-1}$ at 2000 m depth, and 60 $cm.s^{-1}$ at the shallowest level of measurements. Again, in April 2010, deep currents higher than 10 $cm.s^{-1}$ are observed between 1000 m depth and the bottom, but with no surface intensification; thus they are likely related to TRWs.

3.2. Mooring Hydrology

[22] The upper layer variability of the GM is mainly explained by the presence of the LC and LCEs [e.g., *Merrell and Morrison*, 1981; *Brooks and Legeckis*, 1982; *Vukovich and Waddell*, 1991; *Hamilton*, 1992; *Vidal et al.*, 1992; *Hamilton et al.*, 2002; *Vukovich*, 2007]. They are characterized by their warm and saline Subtropical Under Waters (SUW; >22.5°C and >36.5 PSS), originated from the Caribbean Sea and transported within the GM by the LC and LCEs [*Vidal et al.*, 1992]. Thus, the observations of those waters are a good indicator of the anticyclonic LCE and LC features.

[23] At H1 (Figure 3a) in the EGM, the maximum temperature around 150 m depth reaches 26°C, but it decreases to 16°C during July–August 2008 and from mid-August to December 2009. Two other periods of low temperature (below 18°C at 200 m) are observed in early April 2008 and February–March 2009. A concomitant variability in salinity is also observed at 200 m depth during the same period (Figure 4a). The warm waters (>22.5°C) are associated with a maximum of salinity (>36.5 PSS) and cool water (<20°C) with a relative minimum of salinity (<36.00 PSS).

[24] The northward (southward) extension (retraction) of the LC or shedding of LCEs leads to high variability of the water masses present at the site of moorings H1, H2 and H3 and explains the large variability of the temperature (Figure 3a), reaching, for example, a difference of 10°C at the surface between early August 2009 and September 2009 (Figure 3a). The energetic events are mainly associated with periods of strong variations of temperature and salt, as observed between 150 and 600 m depth in early August 2009 or in August 2008, during the retraction/extension of the LC, or the penetration of frontal cool cyclones ('necking'; Figure 3a) into the mooring location.

[25] At P (Figures 3b and 4b, P), the near-surface temperature is about 18°C from October 2008 to mid-May 2009 and increases to about 22°C after June 2009. During early April 2009 an energetic event is associated with a 2°C cooling at 200 m depth due to the presence of a cool cyclone during this period, while the June 2009 event is concomitant with warmer/saltier waters that indicate the crossing of an LCE named DARWIN (name as defined by Horizon Marine Inc., http://www.horizonmarine.com/loop_current_Eddies.php).

[26] At mooring A, the variability of the near-surface temperature is larger than in the northwestern part of the GM (mooring P) ranging from 25°C to 18°C, and the salinity varies from 36.5 to 36.8 PSS (Figures 3c and 4c, A). The warmest and saltiest waters (over 22°C and 36.6 PSS in January–February 2009; August–September 2009; and January–February 2010) are associated with successive LCEs crossings, namely CAMERON (name as defined by Horizon Marine Inc., http://www.horizonmarine.com/loop_current_Eddies.php) during January–February 2009 and DARWIN during April 2009. Thus, the energetic events in February 2009, August–October 2009 are associated with LCEs crossing the mooring site.

[27] In summary, energetic distinct events are observed in several locations and times within the GM. They are characterized by intense, deep flows with an apparent large equivalent barotropic contribution (up to 40 $cm.s^{-1}$ at 2000 m depth), i.e., the flow, although with magnitude varying vertically, is unidirectional from top to bottom [*Gille*, 2003]. They are associated with mesoscale cyclone and anticyclone surface variability that manifests below by strong temperature-

Figure 2. (a) Zonal and (b) meridional velocities (in $cm.s^{-1}$) time series at H1 between near-surface and bottom depth (3300 m) between February 2008 and April 2010. (c) Zonal and (d) meridional velocities (in $cm.s^{-1}$) time series at P between near-surface and bottom depth (3500 m) between September 2008 and July 2010. (e) Zonal and (f) meridional velocities (in $cm.s^{-1}$) time series at A between near-surface and bottom depth (3500 m) between July 2008 and July 2010. Blanks indicate no data. The intermittent deep events are listed in Table 2.

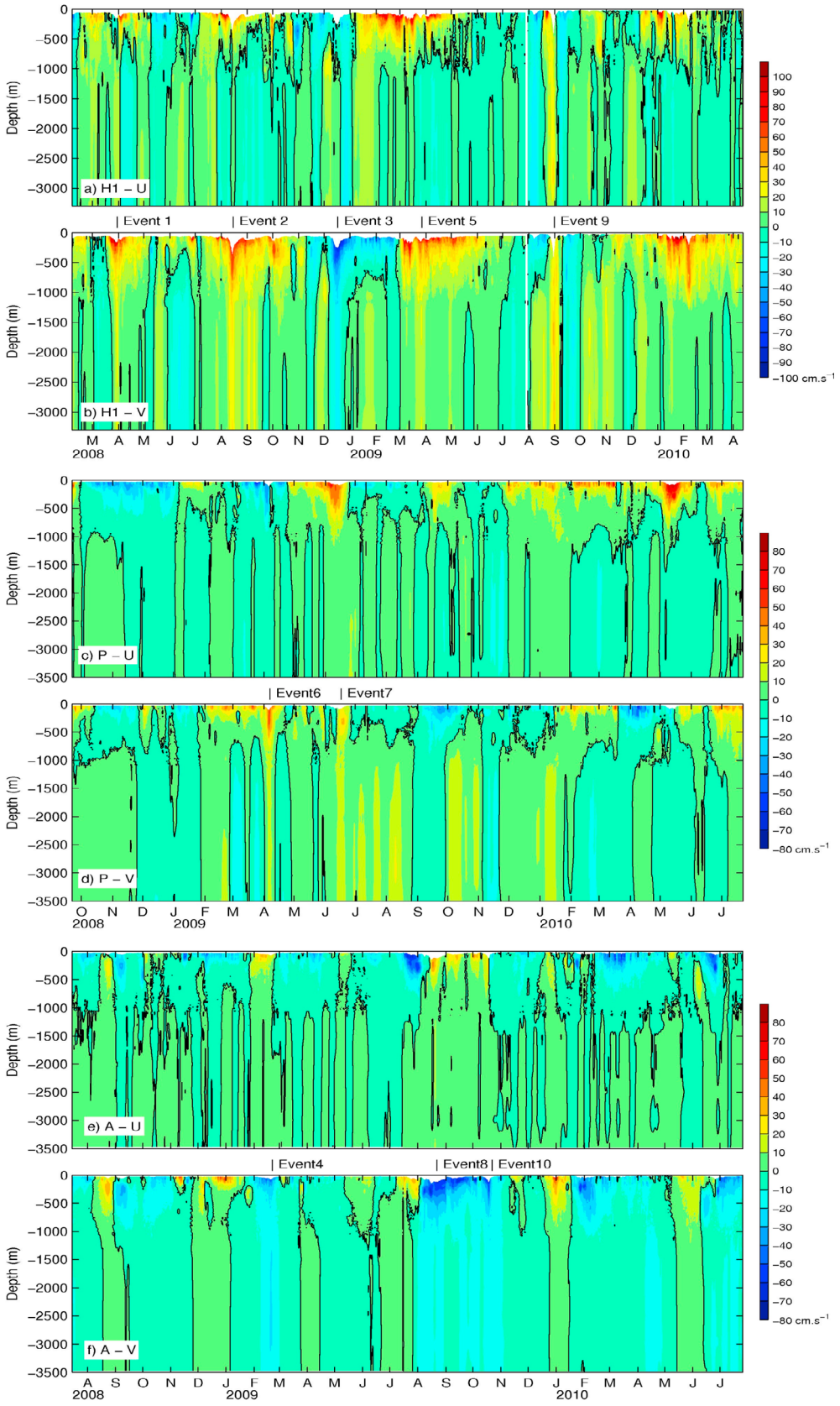
a) H1 – U
b) H1 – V
c) P – U
d) P – V
e) A – U
f) A – V
Depth (m)
| Event 1
| Event 2
| Event 3
| Event 5
| Event 9
| Event6
| Event7
| Event4
| Event8
| Event10
2008
2009
2010
cm.s⁻¹

Figure 2

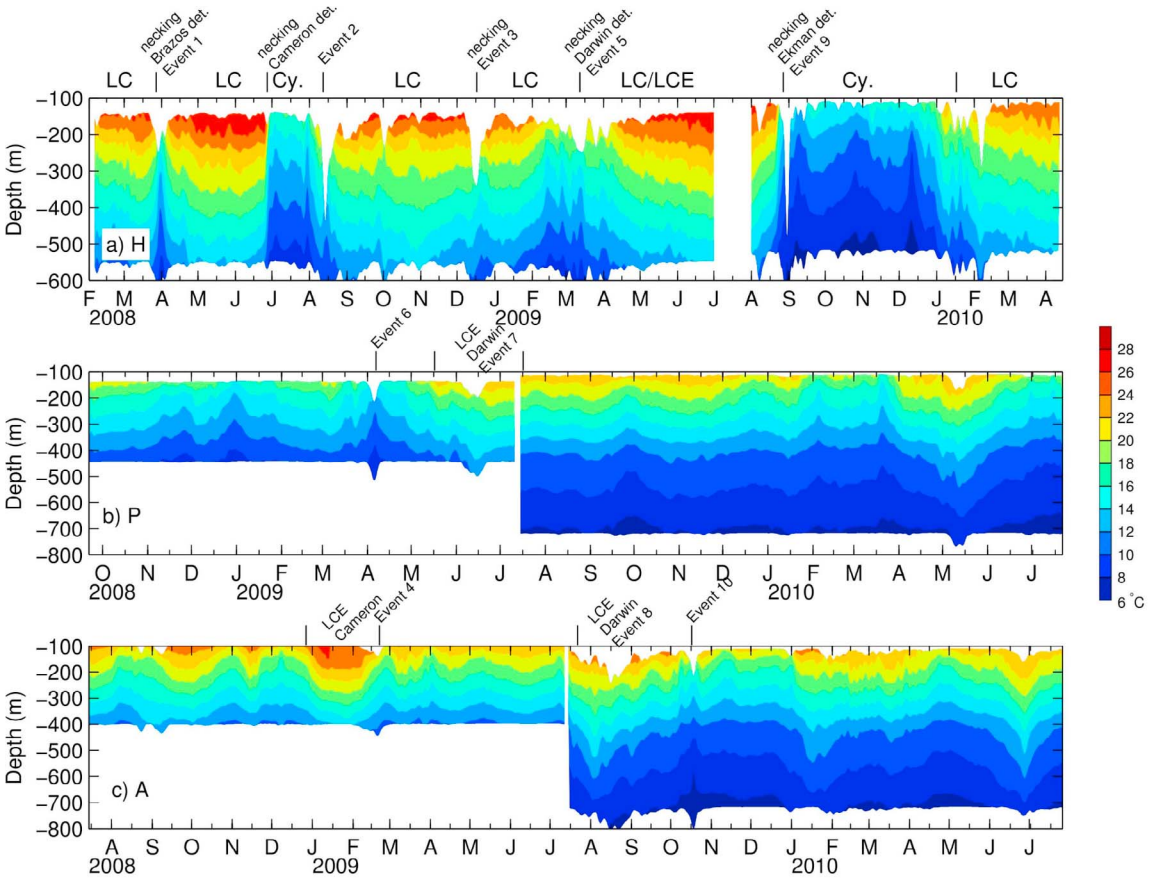

Figure 3. Temperature (in °C) time series at (a) H1 between about 100 and 600 m depth and at (b) P and (c) A between about 100 and 800 m depth. The time range is the same as those for the velocities in Figure 2. Blanks indicate no data. The presence of LCE/LC or cyclonic circulation and separation events identified with altimetry data are indicated at each mooring location. The names of the detached LCEs (Brazos, Cameron, Darwin and Ekman) are defined by Horizon Marine Inc. http://www.horizonmarine.com/loop_current_Eddies.php.

salinity changes in the upper layer with a signature down to 600–800 m depth related to the crossing of the LC or LCEs. The events are more intense in the eastern region, where the surface mesoscale variability is more energetic (LC and LCE shedding, mooring H1), but they also exist on the westward path of LCEs, at moorings A and P.

[28] It is difficult to depict in detail the complete structure of such events from the available mooring data alone. However, these events repeat consistently in the data set. To obtain insight into a potential link with the surface eddy field, the next section shows the surface variability of ADT and the associated surface geostrophic currents in relation with the data from moored instruments.

3.3. Surface Relative Vorticity

[29] The surface geostrophic relative vorticity ($\varsigma = \partial v/\partial x - \partial u/\partial y$, where u and v are the longitudinal and meridional velocity components, x and y are the longitudinal and meridional coordinates) at moorings A, P and H1 is computed and plotted in Figure 5. Surface velocities are deduced from altimetry. At mooring A, during events 4 and 8 (within black lines in Figure 5c) the surface relative vorticity changes from negative to positive values. These changes suggest that the mooring is initially located in surface anticyclonic currents of an LCE, then in a cyclonic circulation. The events (Table 2) occur concomitantly with the changes in sign of the surface vorticity, as, for example, when a dipole-like eddy translates across the mooring (see also Figure 2f). Similar features occur in Figure 5a at mooring H1. The sign change in relative vorticity can be either from positive to negative (events 2 and 5), or vice versa (events 1, 3 and 9) and can be explained by the crossing of the confluence zone between counter rotating flows at the mooring location. In the EGM, such counter rotating flows occur between the LC (or a LCE) and the frontal cyclones surrounding it, in the WGM, between anticyclone-cyclone pairs.

[30] By contrast, Event 10 in Figure 5c and Events 6 and 7 in Figure 5b do not show a change of sign of relative vorticity but show short-term variations of the relative vorticity. From the altimetry data (not shown), moorings A and P were located next to the confluence zone of counter-rotating surface flows during these three events. The mooring was not exactly in the confluence zone of the dipole-like structures and remained in the cyclonic or anticyclonic side (not

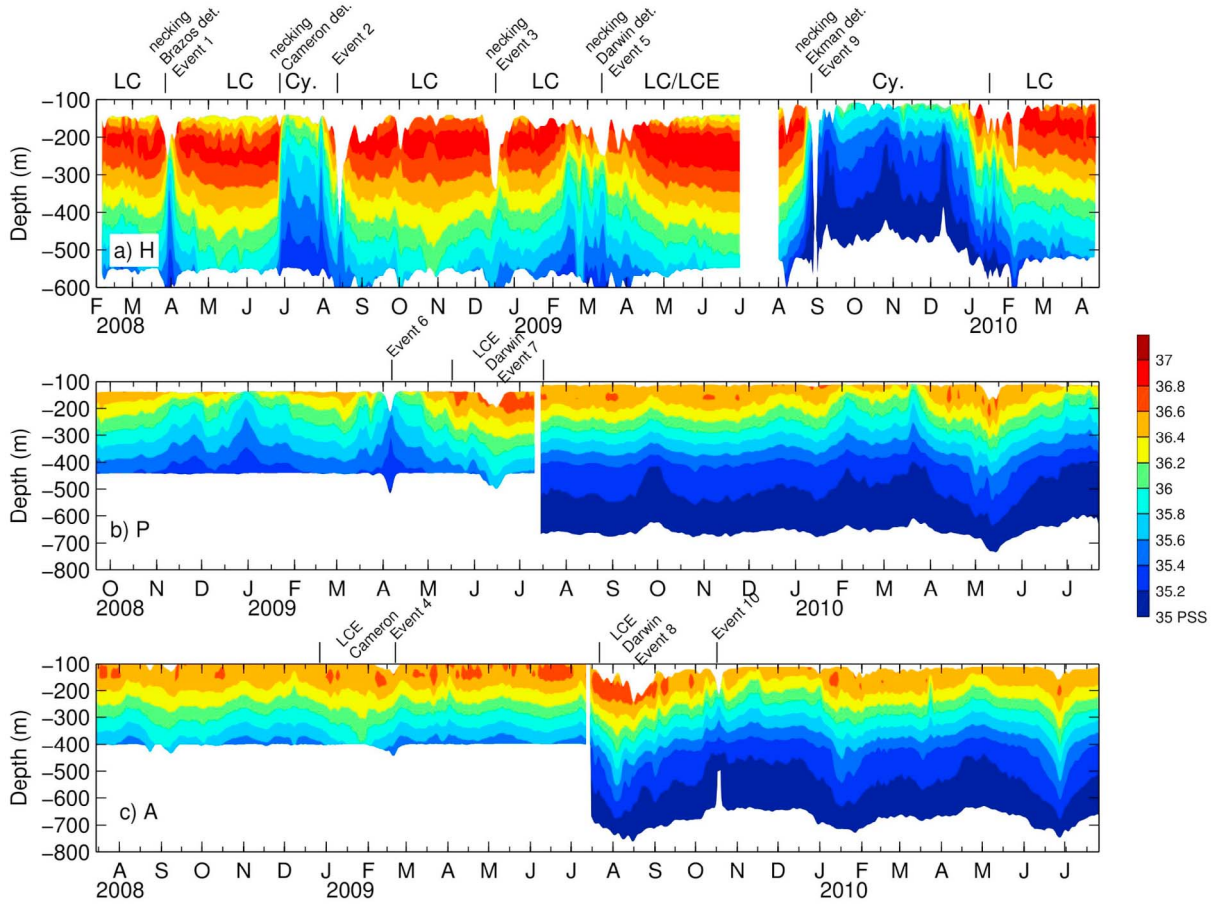

Figure 4. Same as Figure 3 but for salinity (in PSS).

shown). Note also that these events are the weakest of all in the speeds at 2000 m depth (Table 2).

4. Example of Deep, Energetic Events

4.1. Western Gulf of Mexico: Dipole Interaction

[31] Each event has its own peculiarities. In this section, the common features from surface to bottom of the two most striking events in the WGM (events 4 and 8 of Table 2) are described with corresponding Figures 6 and 7.

4.1.1. Event 4, February 2009

[32] On January 20, 2009 (Figure 6a) the intense LCE CAMERON (AC) had a maximum ADT of 1.80 m, a negative relative vorticity of $\sim 1.10^{-5}$ s^{-1} (blue shading), and a near-surface velocity greater than 40 $cm.s^{-1}$ at mooring L. On this date, CAMERON was centered at mooring A (22.5°N–95°W) and had a diameter of about 300 km. Northeast of CAMERON around 24°N–93.5°W, a cyclone (labeled C on Figure 6a) of smaller intensity having 1.20 m of maximum ADT and a maximum swirl velocity of about 20 $cm.s^{-1}$, is evident in the altimetry data. This cyclone is separating from a larger cyclone, centered on 25.5°N–95°W, which extends northward of the anticyclone.

[33] The vertical distribution of velocities at L (Figure 6d) shows close to eastward flows with a clear intensification toward the surface; from less than 5 $cm.s^{-1}$ around 1000 m depth to more than 40 $cm.s^{-1}$ near the surface (~100 m depth). At mooring A (Figure 6g), the velocity, mainly oriented southward but northward at the shallowest level, is weak without exceeding 10 $cm.s^{-1}$ over the full water column. At mooring K, the velocities are southwestward and intensified from 1000 m depth toward the surface, reaching about 50 $cm.s^{-1}$ in the shallowest measurements. Below 1000 m the velocity reverses its direction and remains weak with speeds below 10 $cm.s^{-1}$ down to the bottom. The vertical distribution of the velocities at the three moorings shows the surface intensification during CAMERON's crossing.

[34] On February 19 (Figure 6b), CAMERON has been translating west-southwestward, thus further approaching the western coast, and the smaller C has translated southwestward. The cores of CAMERON and C become closer as those translations take place. Mooring A is now exactly between both eddies: at the confluence of the dipole-like structure. The near-surface velocities have increased (up to 50–60 $cm.s^{-1}$) and are mainly southward following the dipole confluence flux. Through the whole water column, the main velocities are southward and have increased to ~10 $cm.s^{-1}$ at L (Figure 6e) and more than 20 $cm.s^{-1}$ at A (Figure 6h). In Figures 6e and 6h, the velocities exhibit a near-alignment over the vertical, although a small, near-surface deviation of about +13° occurs at L. This feature corresponds to Event 4 listed in Table 2 and observed at A and L during February 2009 (Figure 2c).

[35] From February 19 to March 1 2009, the dipole structure rotated about 45° clockwise. By March 1 2009, eddy C has slowed down (with a maximum swirl velocity of 20 $cm.s^{-1}$), while CAMERON had acquired a bean-shape,

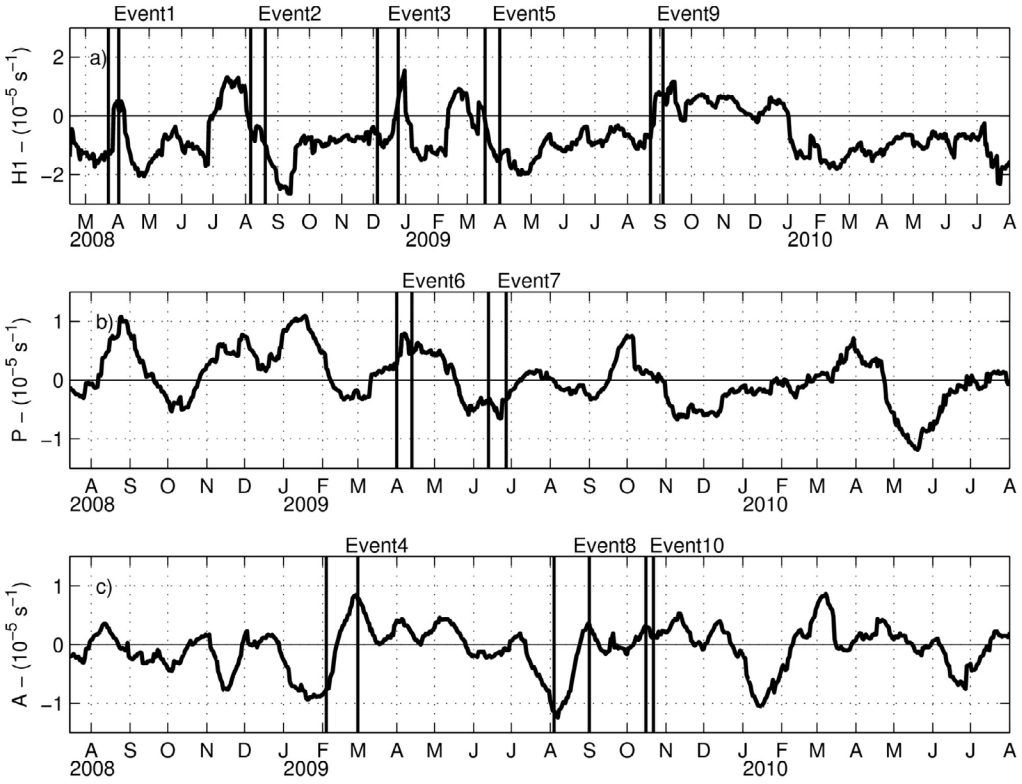

Figure 5. Relative vorticity deduced from the geostrophic currents from AVISO at the location of moorings (a) H1, (b) P and (c) A. The ten deep events listed in Table 2 occur between the solid vertical lines.

probably due to its interactions with the western topography and eddy C. Similar deformations have been reported by various authors [*Vukovich and Waddell*, 1991; *Vidal et al.*, 1992; *Frolov et al.*, 2004; *Hyun and Hogan*, 2008]. At L, the velocities below 1000 m depth were, by this date, about null (Figure 6f), leaving only the near-surface high speeds of 36 cm.s^{-1} oriented southwestward. Mooring A was then on the northern-western edge of C (Figure 6c), with southwestward near-surface velocities of about 19 cm.s^{-1}. At depth, the vertical distribution of velocities was southward, maintaining a speed of about 10 cm.s^{-1} (Figure 6i) suggesting that the cyclone retained a deep signature.

4.1.2. Event 8, August 2009

[36] Six months later, another, deep, energetic event is recorded at moorings L, A and K during the crossing of the LCE DARWIN that interacts also with a companion cyclone (Table 2 and Figure 2c). On July 25 2009, DARWIN with a diameter of about 200 km is located northeast from the L, A and K moorings' area. The southwestern edge of DARWIN swirls across the moorings (Figure 7a). Northeast of DARWIN a cyclone (C) with a ∼170 km diameter is also observed. The vertical distribution of velocities (Figures 7e, 7i and 7m) at each mooring indicates a weakening from the surface up to 1000 m depth. Below 1000 m depth, speeds are not greater than 7 cm.s^{-1} (Figures 7e, 7i and 7m).

[37] On August 5 2009 (Figure 7b), the dipole-like vortex composed of DARWIN-C pair had rotated counter-clockwise and translated southwestward. As during the February 2009 event previously described, DARWIN becomes bean-shaped between the western topography and the eddy C. Mooring L is located near the rear of the dipole axis, while A is near DARWIN's center and K in the southeastern part of DARWIN. At mooring L, located on the northwest side along the dipole axis, the near-surface velocities are southeastward of about 50 cm.s^{-1} (Figure 7f), the velocity turns clockwise and decreases in magnitude toward the bottom reaching about 10 cm.s^{-1} and southward. At mooring A, near the center of DARWIN (Figure 7j) southwestward near-surface velocities greater than 30 cm.s^{-1} decrease toward the deep and below 1000 m the currents remain greater than 15 cm.s^{-1} and almost unidirectional southward. At mooring K (Figure 7n), located in the southeastern region of DARWIN, the surface velocities are westward with speeds reaching 40 cm.s^{-1}, then diminish with depth and reverse, being eastward below 800 m depth.

[38] The cyclonic currents below 1000 m depth, at moorings L, A and K, follow the 3500 m isobath (Figures 7b, 7f, 7j and 7n). In contrast with Event 4, the currents in this event were bottom intensified at the three moorings, and by August 5, no mooring was yet in the dipole's confluence zone, but rather toward DARWIN's core.

[39] On August 19 2009 (Figure 7c), the DARWIN-C dipole had translated southwestward, and moorings L, A and K were now along the dipole-like axis. The near-surface speeds reached more than 50 cm.s^{-1} at mooring L and A (Figures 7f and 7g). Below 1000 m depth, velocities are uniformly aligned over the vertical with speeds greater than 10 cm.s^{-1} at A, although a little smaller than on August 5 2009. In contrast, at L and K (Figures 7g and 7k) the speeds are intensified, reaching 20 cm.s^{-1} at K. The surface

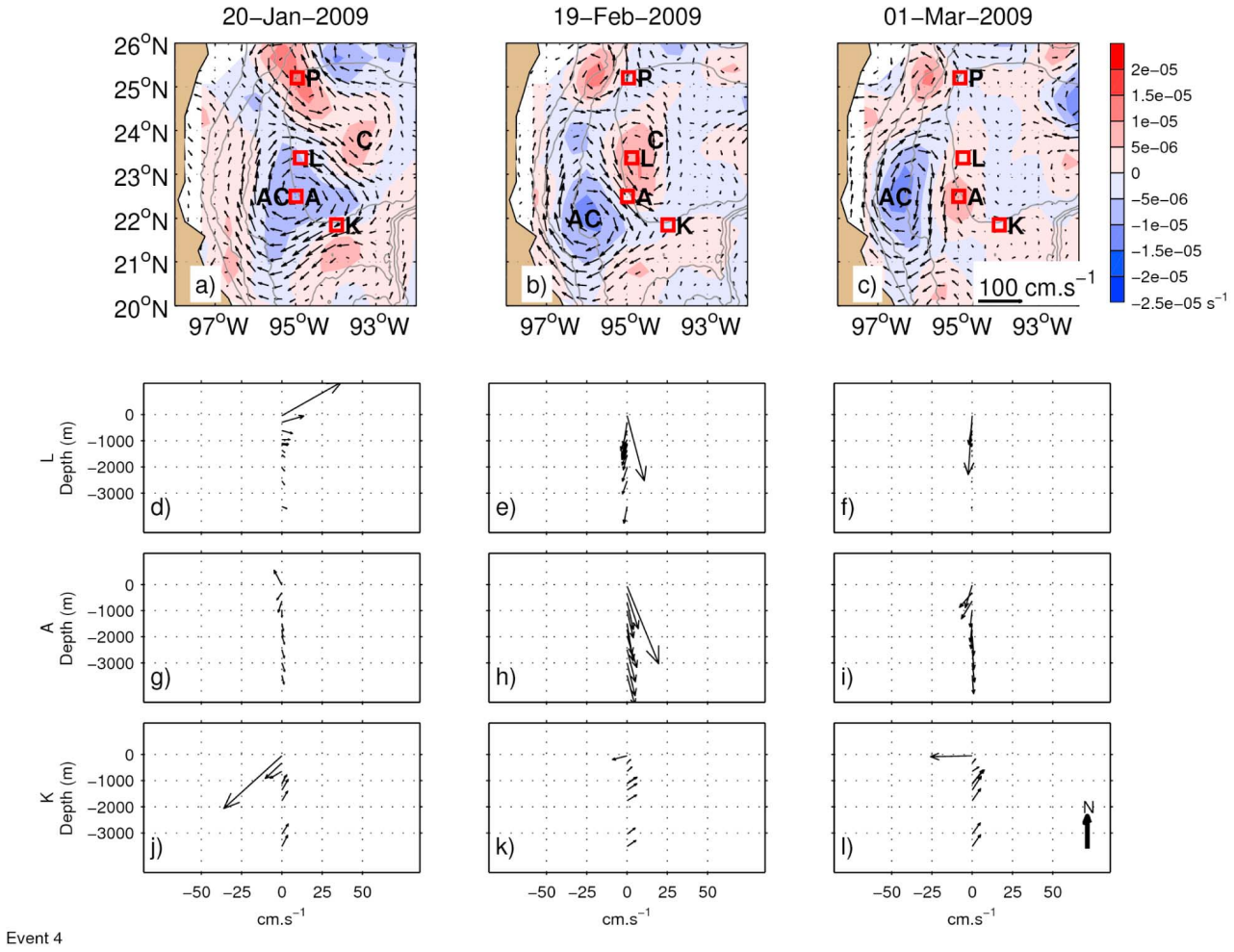

Figure 6. Event 4: (a–c) Geostrophic surface velocities from AVISO (arrows) and relative vorticity computed from surface geostrophic velocities (in s^{-1}; color shading). Red squares are the location of the moorings P, L, A and K. Isobaths are plotted in gray with 1000 m depth intervals from 3500 to 500 m. (d– l) Vertical distribution of horizontal velocities (in cm.s^{-1}) between the near-surface and bottom depth (3500 m depth) at mooring L (Figures 6d–6f), A (Figures 6g–6i) and (Figures 6j–6i). Each column of the figure depicts the surface and subsurface condition corresponding to the date indicated in the title of maps.

velocities were twisted southward (eastward) at K (L). As stated previously, the observation indicates deep layer velocity intensification at moorings A, L and K with a cyclonic circulation along the 3500 m isobath. Moorings L and K are respectively 99 km and 126 km away from A.

[40] By September 5 2009 (Figure 7d), C had dissipated, and DARWIN recovered a circular shape. Mooring A (Figures 7d and 7l), located on the northeastern edge of DARWIN, indicated near-surface speeds of about 40 cm.s^{-1}. At L and A, the speeds below 1000 m have diminished to less than 5 cm.s^{-1} (Figures 7h and 7l), while at K (Figure 7p) the deep speeds are still over 10 cm.s^{-1}, uniform over the vertical and along isobaths.

[41] Event 8 is the second example of energetic events characterized by intense currents over the whole water column with an apparent enhanced barotropic contribution. The alignment of the current occurs at the confluence between two counter-rotating eddies (Figures 6b and 6h for CAMERON and 7c, o for DARWIN), where the velocities of both eddies are in the same direction. However, in contrast with Event 4 (CAMERON), during August 2009 at A (Event 8; DARWIN), the maximum velocities in the lower layer did not occur when the mooring was located at the confluence of the dipole (Figures 6b, 6h, 7c and 7k), but when located within the core of DARWIN. At this moment, the flow was not aligned over the entire water column (Figures 7b and 7j). While DARWIN had a circular shape, possibly when its interaction with C was weak, during the early and last stages of the event (Figures 7a and 7i and Figures 7d and 7l), the velocities in the deep layer were less energetic. *Frolov et al.* [2004] in simplified, two-layer numerical simulations noticed that a surface-trapped, deformed and translating anticyclone causes vertical stretching/compression of the lower layer leading to an increase/decrease of its relative vorticity. This sequence occurs under the interaction of the anticyclone with both the western boundary and a surrounding smaller cyclone and leads to the formation of deep eddies in the lower layer. This behavior is also consistent

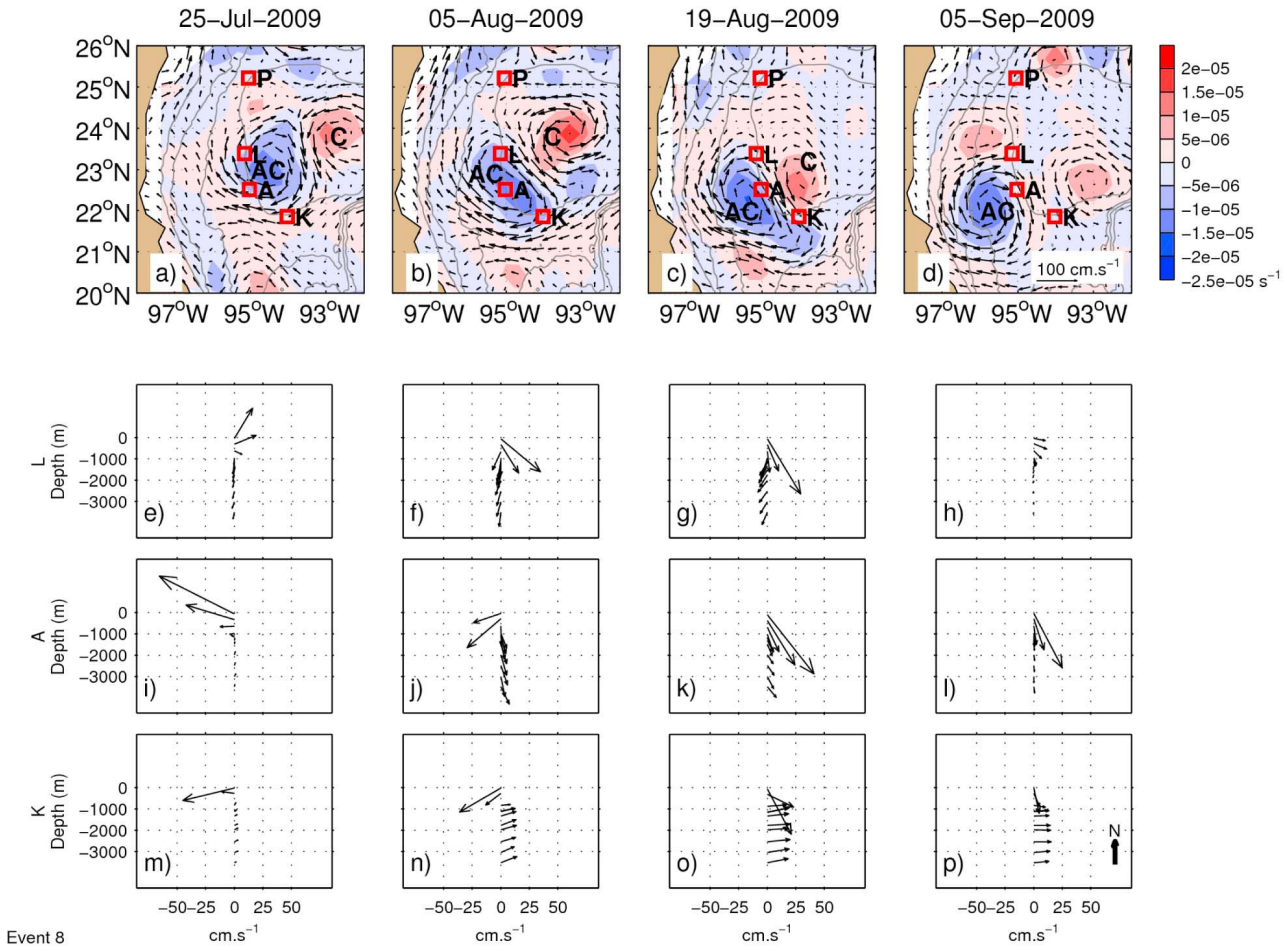

Figure 7. Same as Figure 6 but for event 8.

with the present observations of the intensification of the southward velocities, in early August 2009, that occurred concomitantly with the deformation of DARWIN under the interaction with C. However, in contrast with *Frolov et al.* [2004], during Event 8, the currents were aligned over the vertical during a short time at the location of the confluence zone of the dipole-like vortex (Figure 7k).

4.2. Eastern Gulf of Mexico: Cyclone Interacting With LC and LCE

[42] The EGM and the LCE shedding zone, northwest of the LC, have the most energetic surface mesoscale activity. Here, two examples of deep, energetic events (3 and 9 in Table 2) will be described and discussed in detail.

4.2.1. Event 3, December 2008

[43] On December 5 2008 (Figure 8a), the mooring triangle (H1, H2, H3) was located near the center of an almost shed LCE characterized by a negative relative vorticity and a ~450 km diameter. The LC, also characterized by negative relative vorticity, had its edge retracted east of 87°W and south of 24.5°N. The mooring measurements indicated southwestward near-surface currents (Figures 8a, 8d, 8g and 8j) with speeds between 15 cm.s^{-1} and 30 cm.s^{-1}. The velocities decreased downward, reversing or flowing northeastward just below 800 m at H1 and H3, while it was southeastward at H2. The current speed remained nearly constant, between 11 cm.s^{-1} and 13 cm.s^{-1}. As shown in Figure 2a, the LCE centered at the mooring's location in late-November and early December had a rather strong baroclinic structure, with a flow reversal near 800 m.

[44] On December 15 2008 (Figure 8b), the LCE had been reconnected with the LC, and eastward of the LCE a small cyclone (with positive relative vorticity) appears and 'necks-down' the LCE-LC [*Schmitz*, 2005; *Oey*, 2008]. During Event 3, velocities at the mooring triangle had intensified and aligned in the southward direction over the whole water column (Figures 8e, 8h and 8k). The speeds are between 46(18) cm.s^{-1} and 71(28) cm.s^{-1} near the surface (bottom) at H3 and H2, respectively (Figures 8h and 8k).

[45] On December 25 2008 (Figure 8c), the small cyclone, intensified and approached the LCE core. The deep layer intensification reached 23 cm.s^{-1} and 27 cm.s^{-1} with westward velocities at H1 and H3, but they were not well aligned with the strong surface currents that remained southwestward.

[46] During the development of the cyclone and its translation nearing the LCE, a barotropic intensification of the currents occurred between them, but with a very short duration. After 10 days, the upper and lower layer currents became less aligned, although the speeds remained comparable with those existing during the barotropic intensification.

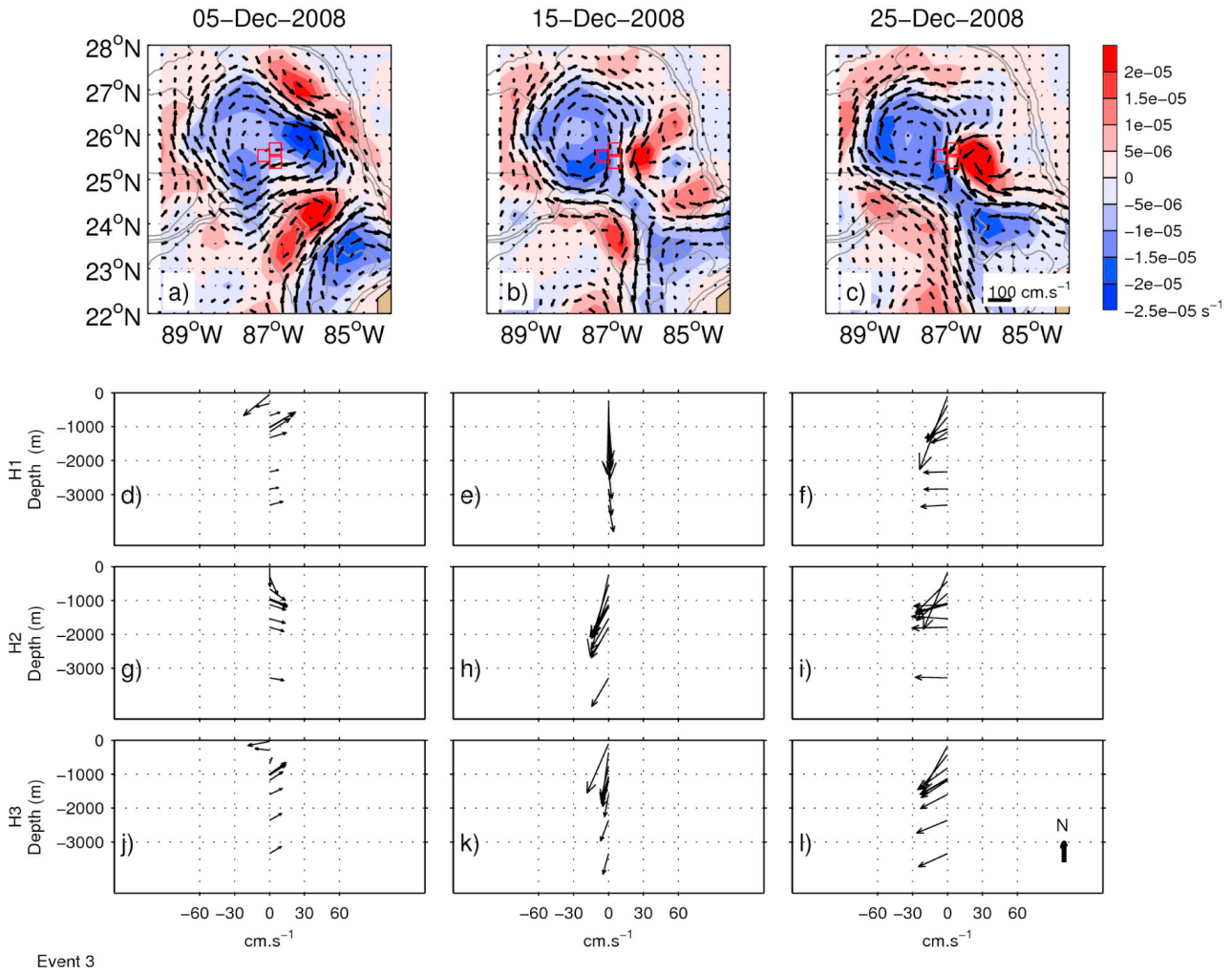

Figure 8. Same as Figure 6 but for event 3.

4.2.2. Event 9, August–September 2009

[47] The AVISO maps from August 15 to September 10 2009 (Figures 9a–9c) show an LCE detachment. Two frontal cyclones, one situated north of the LC, off the western Florida shelf, and another south of the LC, near Campeche Bank, 'necked-down' the LC giving birth to an LCE. The mooring triangle was located near the center of the necking pattern formed by the two frontal cyclones (north and south) and two anticyclones (east and west).

[48] On August 15 2009, the near-surface currents are intensified following the anticyclonic circulation of the twisted LCE (Figure 9a, blue), with velocities varying from 29 cm.s^{-1} to 51 cm.s^{-1} at H3 and H1, respectively (Figures 9d and 9j). Below 800 m depth, the currents are oriented mainly northward with speeds between 12 and 15 cm.s^{-1} (Figures 9g, 9h and 9j). Sixteen days later, on August 31 2009 (Figure 9b), the two cyclones separated the LCE into two anticyclones. The near-surface speeds had now decreased to less than 30 cm.s^{-1} at each mooring location, while the sub-surface and deep speeds had strongly increased to reach 29 cm.s^{-1} and 41 cm.s^{-1} at H2 and H1, respectively (Figures 9e, 9h and 9k). This event was the most intense in its deep manifestation, and occurred during intense upper-layer eddy interaction, but curiously, it differed from the previous events because it was not as intensified at the surface.

[49] On September 10 2009 (Figure 9c), both cyclones had merged, while the eastern fraction of the temporarily detached LCE had merged back, east of 86°W, to the LC. The velocities at the mooring triangle remained uniformly distributed over the vertical (Figures 9f, 9i and 9j) with speeds not greater than 30 cm.s^{-1} except around 1700 m depth at H2 (Figure 9i) and currents rotated westward following the cyclonic circulation of the recently merged cyclone. This most energetic event leads to intense currents in the deep layer, but without the common, much larger, velocities in the upper-layer between the cyclones' cores.

5. Time-Vertical Structure Analysis

5.1. Dynamical Modes

5.1.1. Mooring A

[50] The variability over the water column at mooring A has been projected onto the barotropic and baroclinic normal modes. The normal mode analysis can be justified by the nearly flat bottom topography in the moorings areas. The barotropic and first to fourth baroclinic modes (Figure 10b) were computed from the mean of two full column, high

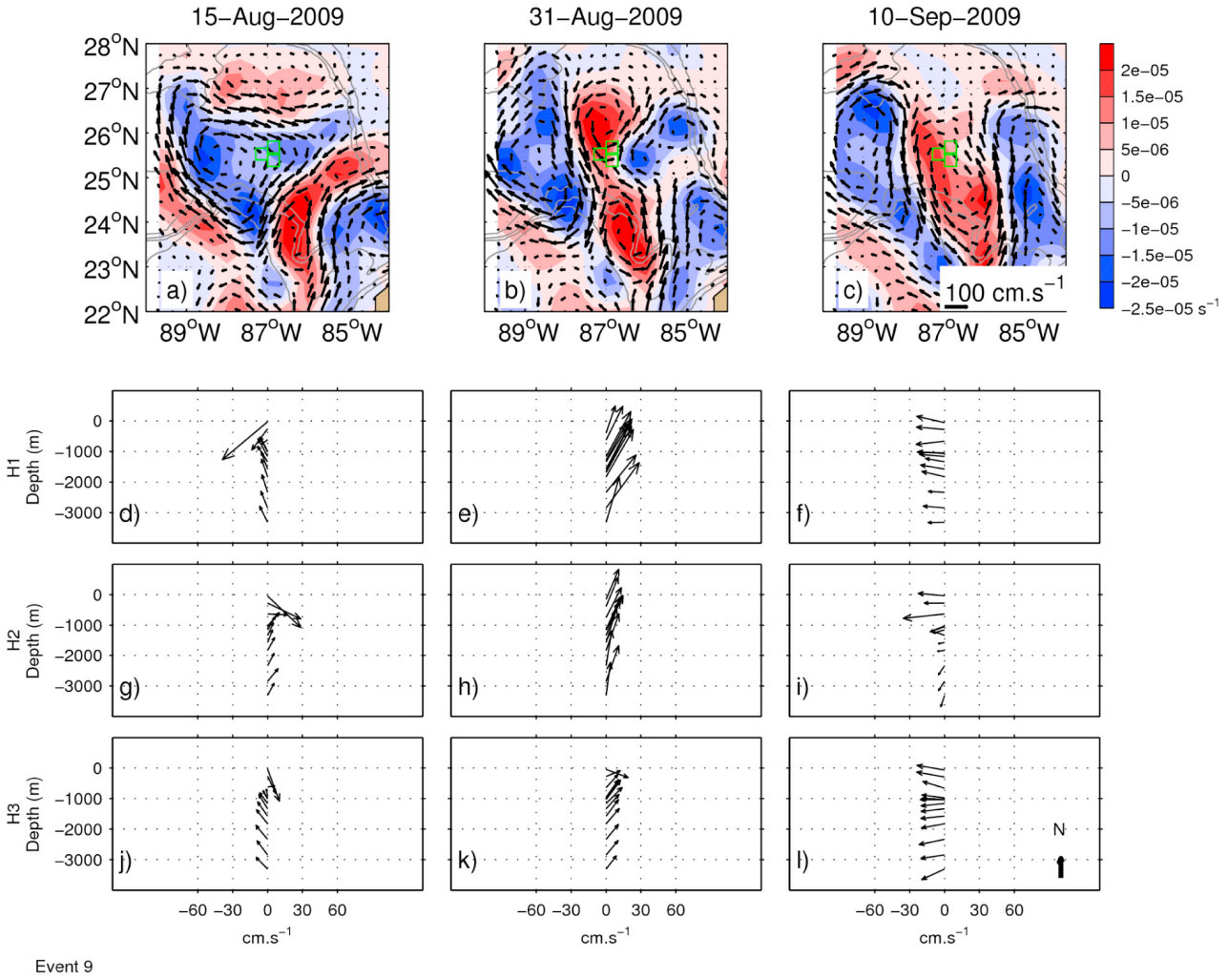

Figure 9. Same as Figure 6 but for event 9.

resolution, hydrographic profiles located near 23°N–91°W (Figure 10a). Both U- and V-components were projected on these modes. The modal decomposition is examined for the U (light gray) and V (dark gray) velocity components (Figure 11). The barotropic and first baroclinic modes capture the largest part of the variability and contribute with 91.7% of the full variance; 55.0% by the barotropic mode and 36.7% by the first baroclinic mode.

[51] Figure 12 (top) presents the time evolution of the amplitudes in cm.s^{-1} of the barotropic and first baroclinic modes for the V-components. Figure 12 (bottom) presents the norm of the barotropic velocity coefficients divided by the norm of the first baroclinic velocity coefficients (black), and its inverse (gray). Such ratios show the dominance of either mode. When, the magnitude of the sum of the barotropic and first baroclinic velocity coefficients is weaker than 5 cm.s^{-1} (Figure 12, top), the results are meaningless for this analysis and therefore removed. The barotropic and first baroclinic modes have comparable amplitudes with the same sign before the January and early August 2009 events (Figure 12, top), during the early stage of an AC crossing the moorings (Figures 6 and 7). The vertical structure of LCEs, with velocities diminishing at depth without reversal, requires significant contributions of the barotropic and first baroclinic modes. The barotropic mode is clearly dominant (black curve Figure 12, bottom) during the events, in particular during the event of February 2009 (vertical solid lines, Figures 12, top and 12, bottom).

[52] On the other hand, during late July 2009, the contribution of the first baroclinic mode was maximum (Figures 12, top and 12, bottom, gray curve, dashed vertical line), and in early September 2009 (last dashed vertical line), the barotropic and first baroclinic modes had comparable amplitudes. During this period, the ACs had circular shapes and, it appears, were weakly interacting with companion cyclones (e.g., C in Figure 7).

5.1.2. Mooring H1

[53] The U- and V-components of the velocities over the water column at H1 mooring have also been decomposed in terms of the barotropic and the lowest four baroclinic normal modes as previously done for mooring A. Figure 13 shows the percentage of the total variance per mode for each component; U in light gray and V in dark gray. The barotropic and first baroclinic modes captured 46.7% and 43.3% of the variance, respectively.

[54] Figure 14 (similar as Figure 12) shows that energetic events (solid vertical lines) occur when the amplitudes in both modes reach a relative extreme. Second, both

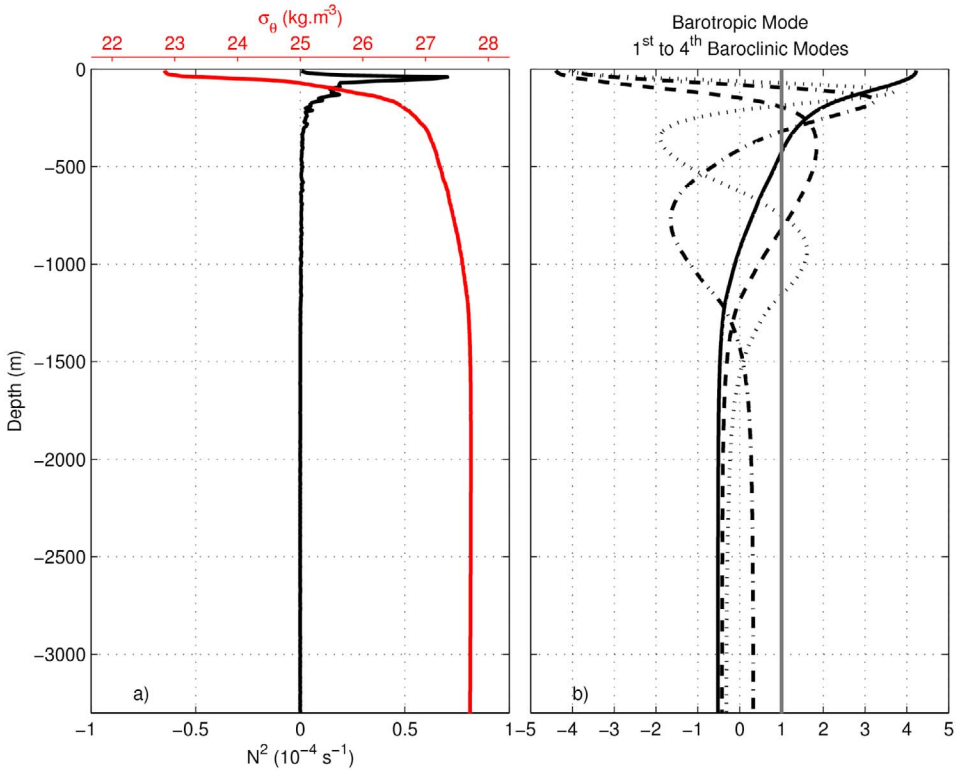

Figure 10. (a) Potential density profile (red) at 23°N–91°W in kg.m^{-3} and Brunt-Väisälä frequency (black) in s^{-1}, from CTD profiles collected near 23°N–91°W. (b) Normalized barotropic (gray) and the four first baroclinic modes (black lines).

amplitudes have comparable values and track each other, revealing the trapping aspect of the surface mesoscale field. The amplitude of the barotropic mode peaks during each event (Figure 14, top). Figure 14 (bottom) indicates that the events (as listed in Table 1) occur during a relative maximum of the ratio of the barotropic amplitude divided by the first baroclinic amplitude (black curve). During late August 2009, this ratio is particularly large (its inverse, in gray curve, was almost null), and characterized the strongest event at H1 (Event 9, Table 2).

5.2. Deep Relative Vorticity Below the LC at Mooring Triangle

[55] The relative vorticity, $\varsigma = \partial v/\partial x - \partial u/\partial y$, is calculated following *Hamilton and Badan* [2009] at fixed-depth levels (z) from the triangle of moored currents measurements by a linear fit to the 5-day low-pass-filtered data

$$u(x,y,z,t) = u_0(z,t) + x \cdot \frac{\partial u}{\partial x}(z,t) + y \cdot \frac{\partial u}{\partial y}(z,t), \qquad (1a)$$

$$v(x,y,z,t) = v_0(z,t) + x \cdot \frac{\partial v}{\partial x}(z,t) + y \cdot \frac{\partial v}{\partial y}(z,t), \qquad (1b)$$

where (x, y) are measured from the center position of the mooring triangle and t is time. $\frac{\partial u}{\partial x}$, $\frac{\partial v}{\partial x}$, $\frac{\partial u}{\partial y}$ and $\frac{\partial v}{\partial y}$ are the functions of depth and time that reproduce via the previous equations the velocity measurements at the mooring's positions. The low-pass-filter reduces noise in what is usually a noisy calculation. The linear fit is essentially averaging ζ over the triangle formed by the moorings as vertices. The relative vorticity has been plotted on Figure 15.

[56] On Figure 15, the energetic events reported in Table 2 are indicated by solid vertical green lines. Near the surface,

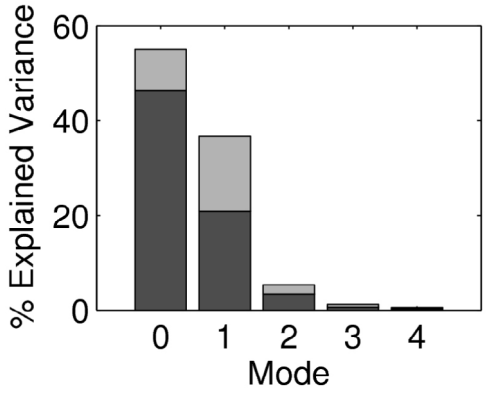

Figure 11. Distribution of the explained variance (in %) for each normal mode and for U- (dark gray) and V-component (light gray) for the velocity time series at A between near-surface and bottom depth between July 2008 and July 2010.

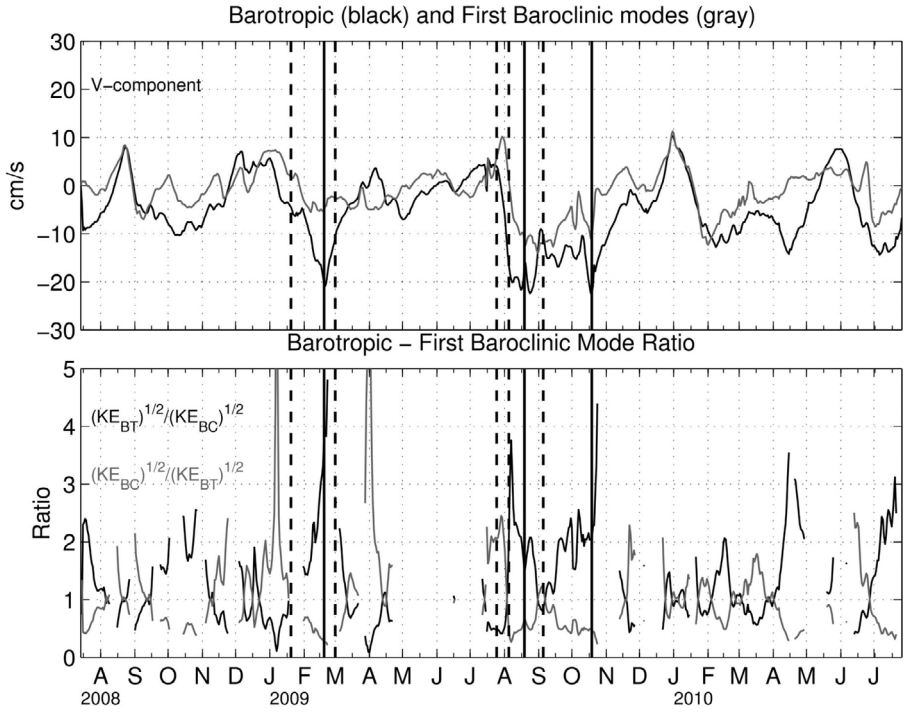

Figure 12. (top) Amplitude time series (in cm.s^{-1}) for barotropic (black curve) and first baroclinic mode (gray curve) for V-component of the velocity time series at A. (bottom) Time series of the barotropic versus baroclinic amplitude ratio (black) and its inverse (gray). The gaps in blank are when the modal amplitudes are lower than 5 cm.s^{-1}, and were removed. The solid vertical lines indicate when the mooring A is exactly at the confluence of a dipole (Figures 6b and 7c for the two first solid vertical lines). The dashed vertical lines indicate the date corresponding to the map of the Figures 6a, 6c, 7a, 7b and 7d.

at 100 m depth, the relative vorticity is negative for most of the observational period; the triangle is in a zone of anticyclonic near-surface currents (LC or LCE). Notice that during February 2009, and from late August to early December 2009, the triangle area is momentarily filled with cyclonic circulation. This pattern is consistent with the cool/fresh signature of cyclones observed during the same period (Figures 3a and 4a).

[57] Below 1000 m, the relative vorticity exhibits strong variability during the events. For example, in mid-August 2008, between 500 m and 3300 m depth, the intensification to the north (Event 2) is concomitant with a bottom-ward increase of relative vorticity, up to a maximum of 0.9 10^{-5} s^{-1}. This intensification of relative vorticity, suggests the presence of a deep cyclone during late August 2008 (Figures 2b and 15). Such intensification was also observed during December 2008 when Event 3 occurred, with a strong intensification of the positive relative vorticity between 100 m depth to the bottom up to 1 10^{-5} s^{-1}. Moreover, during events 2 and 3, the deep intensification of relative vorticity (below 1000 m) leads the near-surface (100 m depth) intensification of the relative vorticity. During Event 5 in late March 2009, only a very weak intensification of the deep relative vorticity occurred (from less than -0.5 10^{-5} s^{-1} to 0 s^{-1} in late March early April 2009).

[58] In late August 2009 (Figure 15, Event 9), an intense, cyclonic, anomaly occurred over the whole water column. The relative vorticity had increased to a maximum value of about 0.5 10^{-5} s^{-1} below 100 m and over 2 10^{-5} s^{-1} near the surface at 100 m depth, with a minimum between 500 and 1000 m depth. Following the same evolution as during events 2 and 3, the increase of deep relative vorticity led (by about 10 days) the near-surface change of sign of relative vorticity, as clearly shown in mid-August 2009, in Figure 15. From September to November 2009 an intense extreme of relative vorticity (up to 0.7 10^{-5} s^{-1}) occurred below 500 m depth, suggesting that the strong, deep currents (Figure 2a) can be explained by deep cyclones and anticyclones.

[59] In summary, in the LC region the relative vorticity analysis shows a supplementary feature associated with the events. In particular, during events 3 and 9, the

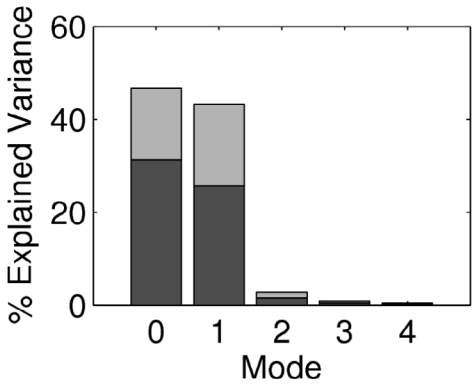

Figure 13. Same as Figure 11 but for the velocity time series at H1.

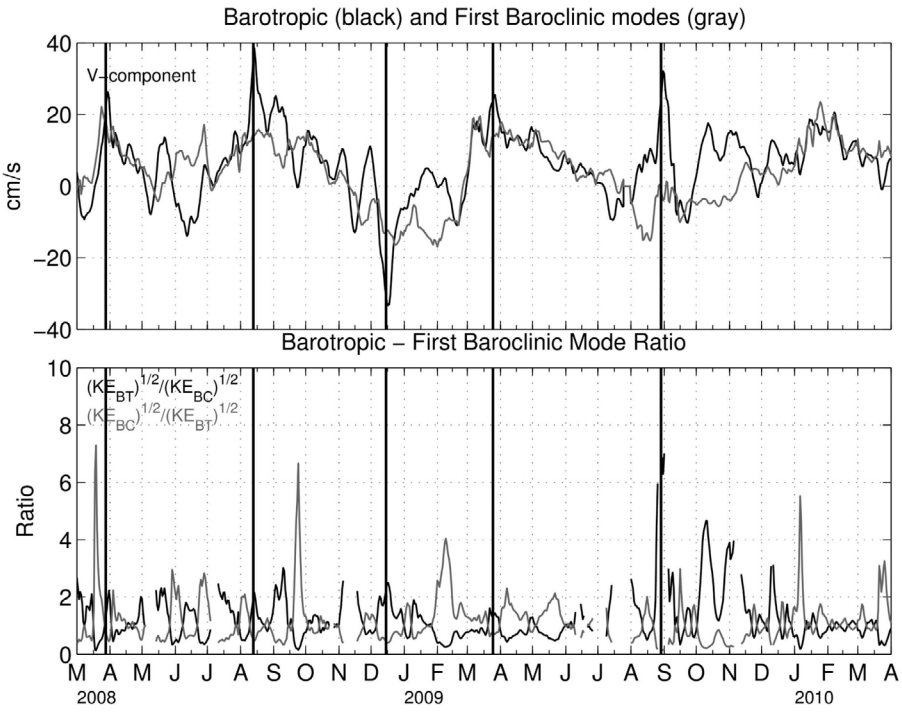

Figure 14. Same as Figure 12 but for the velocity time series at H1.

intensification of relative vorticity occurs first at depth, then at the surface when the frontal cyclone off Campeche Bank and West Florida 'necks' the LC or LCE (see Figures 8 and 9). The increase of deep relative vorticity could be a signature of a deep cyclone in the lower layer of the EGM.

6. Discussion and Conclusion

[60] Observations of velocities in the water column from moorings and surface dynamic height from AVISO show several events characterized by a strong increase in the barotropic or equivalent barotropic contribution of the currents. These events are associated with a prominent deepening of moored instruments. In the LC region, where the most intense events were found, the deepening reached up to 350 m for the shallowest instrumented buoy, designed to sit close to 100 m below the surface. In the WGM, the deepening of the shallowest instrumented buoy reached close to 90 m. The deepening of buoys is due to the drag that sways the mooring line from its vertical standing. The intense deepening or drawdowns occur when the drag, coming from the horizontal currents, has uniform direction throughout the water column, as due to barotropic or equivalent barotropic currents. Currents with a large barotropic or equivalent barotropic contribution occur at the confluence region between counter-rotating flows. In all the events within the EGM, the concomitant presence of intensified deep cyclones is suggested.

[61] Two types of events in the WGM have been discussed. In both types, they are the manifestation of a barotropic central intermittent intensified current occurring in the middle of a dipole vortex as previously reported by *de Ruijter et al.* [2004] near the South Madagascar Current.

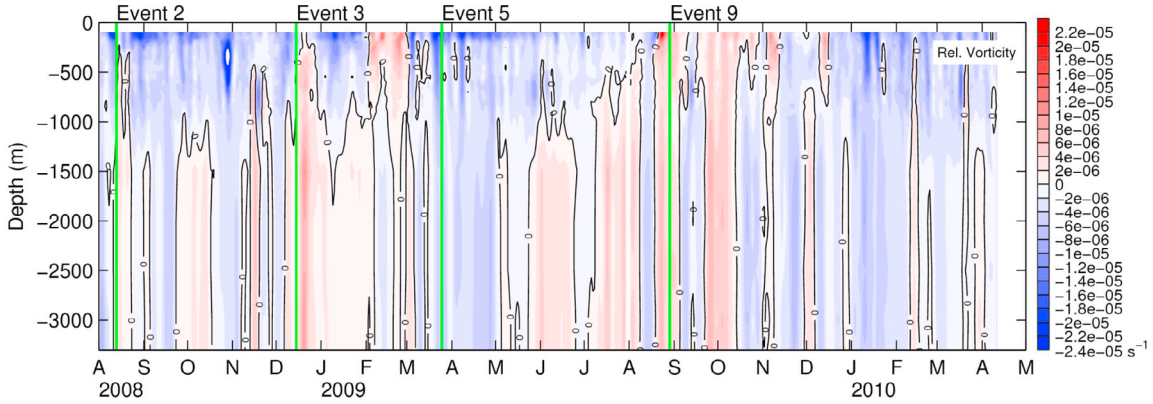

Figure 15. Time series of relative vorticity (in s^{-1}) computed from H1, H2 and H3 velocity time series from 100 to 3300 m depth between August 2008 and April 2010. Solid green vertical lines indicate the date of the events listed in the Table 2.

In the EGM, in the region of the LC penetration, the barotropic intensified currents are observed between two counter-rotating eddies or between the anticyclonic circulation of the LC and surrounding frontal cyclones.

[62] The dynamical vertical mode analysis shows that, during the events, there is an enhanced coherence between the upper and lower layer currents, manifested by an increased contribution of the barotropic mode. The lower layer is driven, most of the time, by mechanisms independent of the surface LC and LCEs [*Sturges and Leben*, 2000; *Oey*, 1996, 2008; *Welsh and Inoue*, 2000; *Ramanou et al.*, 2004; *Chérubin et al.*, 2006]. As suggested here, an increased contribution in the barotropic mode of the currents is the result of the interaction of surface eddies or counter-rotating flows. Previous works have noticed such kinds of events up to 1000 m depth [*Cochrane*, 1972; *Vukovich*, 1986; *Vukovich and Maul*, 1985; *Zavala-Hidalgo et al.*, 2003; *Schmitz*, 2005]. *Inoue et al.* [2008] have observed with a 3-yearlong moored array of current meters in the LC region similar energetic events, with a phase-locking over the vertical (their events 2 and 3). With altimetry data, they show that these deep, energetic events appear during the LC tip separation. On their Figures 3–15 to 3–18, the altimetry data show the LC 'necking', dominantly due to a cyclone. Their observations are consistent with the events studied here in the LC region, where surrounding cyclones come into play.

[63] The existence of the intermittent, deep, intensified currents described opens many questions. The intensification of the flow between counter-rotating flows is expected by the conservation of transport when convergence occurs. The interaction of surface eddies or convergence of counter-rotating flows is not rare. In the events here described, however, the deep extension of the intensification remains unclear in origin and nature.

[64] Different causes could be responsible for such features. The AC that crosses the mooring area in event 4 is obvious surface-trapped, without any aligned flow at depth, before or after the event, and it is plausible that the Cs have a more barotropic structure than the ACs, as observed in the EGM (Figure 15) during events 3 and 9.

[65] Therefore, the evidence of the deep intensification and alignment as a result of nearing the cores of surface counter-rotating eddies is not conclusive; it does not show in all cases. From potential vorticity conservation, the stretching of the lower layer, below the path of a surface trapped anticyclone, contributes probably to an intensification of the deep circulation that induces a larger contribution of the barotropic mode (event 8).

[66] It is plausible that the interaction of the ACs with cyclones could force velocities in the layer below with a barotropization tendency [*Rhines*, 1977, 1979], when surface and deep underlying eddies tend to become locked to each other over the vertical. However, in the EGM, the relative vorticity shows a 10-day delay in the upper layer relative to the lower layer. This delay is in agreement with a baroclinic instability process; given the expected 90° phase difference [*Hurlburt and Thompson*, 1980; *Chérubin et al.*, 2006], the periodicity of the LC/LCE frontal meanders should be ~40 days. Under this scenario, the lower layer eddies/waves lead and do not coincide with the surface perturbations of the front. Therefore, the perturbations are only occasionally aligned over the vertical. This strong relative vorticity signal may not be as important in the WGM.

[67] *Hamilton* [2007] reveals that TRWs can be observed up to the surface. Nevertheless, at the mooring triangle and other mooring locations, the bottom topography is nearly flat. Thus, interaction with a sloping bottom is not a requisite.

[68] These observations (of intermittent, intense, deep currents) suggest that the transmission of energy from the upper to deep layer occurs through the interaction of mesoscale eddies dominantly residing in the upper layer. Indeed, deep eddies are also suggested in the present data. In the WGM, during August 2009 the currents at moorings L, A and K illustrate intensification of cyclonic circulation (Figure 7), concomitantly with the crossing of the LCE DARWIN and the interaction between DARWIN and a cyclone. *Hurlburt and Thompson* [1982], in a two layer model of the GM, demonstrated that the westward translation of LCEs under the beta effect was associated with deep 'modons': a pair of eddies constituted by a deep anticyclone ahead of the LCE and a deep cyclone at its rear. The coupling of this modon with the surface LCE, as explained by *Cushman-Roisin et al.* [1990], results from the compression/stretching of the lower layer ahead/behind the LCE trajectory. *Hurlburt and Thompson* [1982] also found a rapid dissipation of the anticyclone and an enhancement of the deep cyclone in their numerical experiments. *Frolov et al.* [2004] show that a moving, deformed, surface-trapped eddy generates eddies in the lower layer. This mechanism can be a cause of enhancement of deep cyclonic circulation during the interaction of DARWIN in August 2009. *Welsh and Inoue* [2000], using a primitive equations model of the GM, have shown also that the deep eddies tend to be constrained by the bottom topography, and contribute to force TRWs [*Kolodziejczyk et al.*, 2011].

[69] The increase of kinetic energy and positive vorticity in the deep layer of the EGM suggests the presence of deep cyclones, particularly when frontal cyclones interact with the LC or LCEs, mainly during the 'necking-down' process as defined by *Schmitz* [2005]. One of such events is remarkably obvious during August 2009, as characterized by high cyclonic relative vorticity in the lower layer. This feature suggests the passage of a cyclone in the lower layer, generated under the LC [*Inoue et al.*, 2008].

[70] With the use of a high resolution (grid size 5–2 km) numerical model, *Oey* [2008] describes a standard scenario for LC eddy shedding. Basically, after an extension phase of the LC into the GM, a frontal cyclone located off Florida penetrates into the LC extension, intensifies at depth and then cleaves the LC developing the 'necking' [*Schmitz*, 2005; *Oey*, 2008, Figure 3]. According to *Oey* [2008], this scenario involves a baroclinic instability process that intensifies a deep cyclone beneath the LC. The scenario of *Oey* [2008] is discussed for the LC extension and ring shedding, but the 'necking' is not exclusive of the LC as it does occur, also, in the subdivision of an already detached LCE [*Chérubin et al.*, 2006]. The present observations are consistent with the scenario of *Oey* [2008], suggesting an intensification of a deep cyclone below the LC shortly before the 'necking-down' of the LC. In the present data, it

is a LCE that is 'necked' by frontal cyclones. These observations add details to a consistent set of features within this scenario. First, a noticeable rise of positive relative vorticity at depth propagates from the deep layer to the surface during the 'necking phase' which can end up with LCE shedding [*Chérubin et al.*, 2006; *Oey*, 2008]. Second, interaction of the frontal and deep cyclones with the LCE is associated with a barotropic intensification of the currents.

[71] Intermittent, intense, deep currents have been described in view of moored (hydrographic and current) observations and satellite altimetry in the GM. These intense currents occur as deduced by altimetry, at the confluence region between counter-rotating flows when the surface convergence of the flow is in agreement with the surface intensification, and have a large contribution from the barotropic mode. In the EGM, these intensified barotropic currents and the 'necking' of the LC or LCE are associated with the increase of positive relative vorticity in the deep layer. In the WGM, deep cyclonic circulation is associated with the crossing of surface-trapped LCEs interacting with cyclones.

[72] **Acknowledgments.** Data acquisition and analysis were financed by Convenio PEMEX PEP-CICESE 428229851, Medición y Análisis Metoceánico del Golfo de México Etapa 2009 2013. The authors thank Xavier Capet, Claire Menesguen, Bach-Lien Hua and Xavier Carton for very helpful discussions regarding these observations, and Chris Mooers and anonymous reviewers for their corrections and comments that substantially improve the manuscript.

References

Brooks, D. A., and R. V. Legeckis (1982), A ship and satellite view of hydrographic features in the western Gulf of Mexico, *J. Geophys. Res.*, *87*(C6), 4195–4206, doi:10.1029/JC087iC06p04195.

Chérubin, L. M., Y. Morel, and E. P. Chassignet (2006), Loop Current ring shedding: The formation of cyclones and the effect of topography, *J. Phys. Oceanogr.*, *36*, 569–591, doi:10.1175/JPO2871.1.

Cochrane, J. D. (1972), Separation of an anitcyclone and subsequent development in the Loop Current (1969), in *Contributions on the Physical Oceanography of the Gulf of Mexico*, edited by L. R. A. Capurro and J. L. Reid, pp. 91–106, Gulf Publ., Houston, Texas.

Cushman-Roisin, B., E. P. Chassignet, and B. Tang (1990), Westward motion of mesoscale eddies, *J. Phys. Oceanogr.*, *20*, 758–768, doi:10.1175/1520-0485(1990)020<0758:WMOME>2.0.CO;2.

DeHaan, C. J., and W. Sturges (2005), Deep cyclonic circulation in the Gulf of Mexico, *J. Phys. Oceanogr.*, *35*, 1801–1812, doi:10.1175/JPO2790.1.

de Ruijter, W. P., H. M. van Aken, E. J. Beier, J. R. E. Lutjeharms, R. P. Matano, and M. W. Schouten (2004), Eddies and dipoles around South Madagascar: Formation, pathways and large-scale impact, *Deep Sea Res., Part I*, *51*, 383–400, doi:10.1016/j.dsr.2003.10.011.

Frolov, S. A., G. G. Sutyrin, G. D. Rowe, and L. M. Rothstein (2004), Loop Current eddy interaction with the western boundary in the Gulf of Mexico, *J. Phys. Oceanogr.*, *34*, 2223–2237, doi:10.1175/1520-0485(2004)034<2223:LCEIWT>2.0.CO;2.

Gille, S. T. (2003), Float observations of the Southern Ocean. Part I: Estimating mean fields, bottom velocities, and topographic steering, *J. Phys. Oceanogr.*, *33*, 1167–1181, doi:10.1175/1520-0485(2003)033<1167:FOOTSO>2.0.CO;2.

Hamilton, P. (1990), Deep currents in the Gulf of Mexico, *J. Phys. Oceanogr.*, *20*, 1087–1104, doi:10.1175/1520-0485(1990)020<1087:DCITGO>2.0.CO;2.

Hamilton, P. (1992), Lower continental slope cyclonic eddies in the central Gulf of Mexico, *J. Geophys. Res.*, *97*(C2), 2185–2200, doi:10.1029/91JC01496.

Hamilton, P. (2007), Deep-current variability near the Sigsbee Escarpment in the Gulf of Mexico, *J. Phys. Oceanogr.*, *37*, 708–726, doi:10.1175/JPO2998.1.

Hamilton, P. (2009), Topographic Rossby waves in the Gulf of Mexico, *Prog. Oceanogr.*, *82*, 1–31, doi:10.1016/j.pocean.2009.04.019.

Hamilton, P., and A. Badan (2009), Subsurface jets in the northern Gulf of Mexico, *J. Phys. Oceanogr.*, *39*, 2875–2891, doi:10.1175/2009JPO4158.1.

Hamilton, P., T. J. Berger, and W. Johnson (2002), On the structure and motions of cyclones in the northern Gulf of Mexico, *J. Geophys. Res.*, *107*(C12), 3208, doi:10.1029/1999JC000270.

Hofmann, E. E., and S. J. Worley (1986), An investigation of the circulation of the Gulf of Mexico, *J. Geophys. Res.*, *91*, 14,221–14,236, doi:10.1029/JC091iC12p14221.

Hurlburt, H. E., and J. D. Thompson (1980), A numerical study of Loop Current intrusions and eddy shedding, *J. Phys. Oceanogr.*, *10*, 1611–1651, doi:10.1175/1520-0485(1980)010<1611:ANSOLC>2.0.CO;2.

Hurlburt, H. E., and J. D. Thompson (1982), The dynamics of the Loop Current and shed eddies in a numerical model of the Gulf of Mexico, in *Hydrodynamics of the Semi-Enclosed Seas*, *Elsevier Oceanogr. Ser.*, vol. 34, edited by J. C. J. Nihoul, pp. 243–297, Elsevier Sci., New York, doi:10.1016/S0422-9894(08)71247-9.

Hyun, K. H., and P. J. Hogan (2008), Topographic effects on the path and evolution of Loop Current eddies, *J. Geophys. Res.*, *113*, C12026, doi:10.1029/2007JC004155.

Inoue, M., S. E. Welsh, and L. J. Rouse Jr, and E. Weeks (2008), Deepwater currents in the eastern Gulf of Mexico: Observations at 25.5°N and 87°W, *OCS Study MMS 2008–01*, Gulf of Mex. OCS Reg., Miner. Manage. Serv., U.S. Dep. of the Inter., New Orleans, La.

Kolodziejczyk, N., J. Ochoa, J. Candela, and J. Sheinbaum (2011), Deep current in the Bay of Campeche, *J. Phys. Oceanogr.*, *41*, 1902–1920, doi:10.1175/2011JPO4526.1.

Merrell, W. J., Jr., and M. Morrison (1981), On the circulation of the western Gulf of Mexico with observations from April 1978, *J. Geophys. Res.*, *86*(C5), 4181–4185, doi:10.1029/JC086iC05p04181.

Oey, L.-Y. (1996), Simulation of mesoscale variability in the Gulf of Mexico: Sensitivity studies, comparison with observations, and trapped wave propagation, *J. Phys. Oceanogr.*, *26*, 145–175, doi:10.1175/1520-0485(1996)026<0145:SOMVIT>2.0.CO;2.

Oey, L.-Y. (2008), Loop Current and deep eddies, *J. Phys. Oceanogr.*, *38*, 1426–1449, doi:10.1175/2007JPO3818.1.

Oey, L.-Y., and H.-C. Lee (2002), Deep eddy energy and topographic Rossby waves in the Gulf of Mexico, *J. Phys. Oceanogr.*, *32*, 3499–3527, doi:10.1175/1520-0485(2002)032<3499:DEEATR>2.0.CO;2.

Oey, L.-Y., T. Ezer, and H.-C. Lee (2005), Loop Current, rings and related circulation in the Gulf of Mexico: A review of numerical models and future challenges, in *Circulation in the Gulf of Mexico: Observation and Models*, *Geophys. Monogr. Ser.*, vol. 161, edited by W. Sturges and A. Lugo-Fernandez, pp. 31–56, AGU, Washington, D. C.

Ramanou, A., E. P. Chassignet, and W. Sturges (2004), Gulf of Mexico circulation within a high-resolution numerical simulation of the North Atlantic Ocean, *J. Geophys. Res.*, *109*, C01003, doi:10.1029/2003JC001770.

Rhines, P. B. (1970), Edge-, bottom-, and Rossby waves in a rotating stratified fluid, *Geophys. Fluid Dyn.*, *1*, 273–302, doi:10.1080/03091927009365776.

Rhines, P. B. (1977), The dynamics of unsteady currents, in *The Sea*, vol. 6, edited by E. A. Goldberg et al., pp. 189–318, John Wiley, New York.

Rhines, P. B. (1979), Geostrophic turbulence, *Annu. Rev. Fluid Mech.*, *11*, 401–441, doi:10.1146/annurev.fl.11.010179.002153.

Rio, M.-H., and F. Hernandez (2004), A mean dynamic topography computed over the world ocean from altimetry, in situ measurements, and a geoid model, *J. Geophys. Res.*, *109*, C12032, doi:10.1029/2003JC002226.

Schmitz, W. J., Jr. (2005), Cyclones and westward propagation in the shedding of anticyclonic rings from the Loop Current, in *Circulation in the Gulf of Mexico: Observations and Models*, *Geophys. Monogr. Ser.*, vol. 161, edited by W. Sturges and A. Lugo-Fernandez, pp. 241–261, AGU, Washington, D. C.

Smith, S. K., and G. K. Vallis (2001), The scales and equilibration of mid-ocean eddies: Freely evolving flow, *J. Phys. Oceanogr.*, *31*, 554–571, doi:10.1175/1520-0485(2001)031<0554:TSAEOM>2.0.CO;2.

Smith, S. K., and G. K. Vallis (2002), The scales and equilibration of mid-ocean eddies: Forced dissipative flow, *J. Phys. Oceanogr.*, *32*, 1699–1720, doi:10.1175/1520-0485(2002)032<1699:TSAEOM>2.0.CO;2.

Sturges, W., and R. Leben (2000), Frequency of ring separations from the loop current in the Gulf of Mexico: A revised estimate, *J. Phys. Oceanogr.*, *30*, 1814–1819, doi:10.1175/1520-0485(2000)030<1814:FORSFT>2.0.CO;2.

Vidal, V. M. V., F. V. Vidal, and J. M. Pérez-Molero (1992), Collision of a Loop Current anticyclonic ring against the continental shelf slope of the Western Gulf of Mexico, *J. Geophys. Res.*, *97*(C2), 2155–2172, doi:10.1029/91JC00486.

Vukovich, F. M. (1986), Aspects of the behavior of cold perturbations in the eastern Gulf of Mexico: A case study, *J. Phys. Oceanogr.*, *16*, 175–188, doi:10.1175/1520-0485(1986)016<0175:AOTBOC>2.0.CO;2.

Vukovich, F. M. (2007), Climatology of the ocean features in the Gulf of Mexico using satellite remote sensing data, *J. Phys. Oceanogr.*, *37*, 689–707, doi:10.1175/JPO2989.1.

Vukovich, F. M., and G. A. Maul (1985), Cyclonic eddies in the eastern Gulf of Mexico, *J. Phys. Oceanogr.*, *15*, 105–117, doi:10.1175/1520-0485(1985)015<0105:CEITEG>2.0.CO;2.

Vukovich, F. M., and E. Waddell (1991), Interaction of a warm ring with the western slope in the Gulf of Mexico, *J. Phys. Oceanogr.*, *21*, 1062–1074, doi:10.1175/1520-0485(1991)021<1062:IOAWRW>2.0.CO;2.

Welsh, S. E., and M. Inoue (2000), Loop Current rings and the deep circulation in the Gulf of Mexico, *J. Geophys. Res.*, *105*(C7), 16,951–16,959, doi:10.1029/2000JC900054.

Wunsch, C. (1997), The vertical partition of oceanic horizontal kinetic energy, *J. Phys. Oceanogr.*, *27*, 1770–1794, doi:10.1175/1520-0485(1997)027<1770:TVPOOH>2.0.CO;2.

Zavala-Hidalgo, J., S. L. Morey, and J. J. O'Brien (2003), Cyclonic eddies northeast of the Campeche Bank from altimetry data, *J. Phys. Oceanogr.*, *33*, 623–629, doi:10.1175/1520-0485(2003)033<0623:CENOTC>2.0.CO;2.